Journal of Materials Chemistry A

ROYAL SOCIETY OF CHEMISTRY

PAPER

View Article Online
View Journal | View Issue

Cite this: J. Mater. Chem. A, 2025, 13, 29120

Bio-based vinylogous urethane vitrimers from waste-wood lignosulfonate and enzymatic lignin: explorations in stress relaxation behavior and mechanical strength†

Florian C. Klein, [a] Nils Sobania [a] and Volker Abetz *[ab]

Lignin is one of the most promising materials for a biocircular economy. It is not only the most abundant biomaterial, but it has also gathered significant interest in both academia and industry as a new feedstock for plastics. Lignin is primarily produced as a byproduct in the pulping industry, but it can also be extracted from lignocellulosic biomass contributing to waste-wood valorization. The combination with thermomechanical reprocessable polymers, such as vitrimers, enables the synthesis of thermosetting materials with high mechanical strength that can be reused. Herein, we present catalyst-free vinylogous urethane vitrimers based on lignosulfonate and enzymatic lignin, using a commercial bio-based diamine and a bio-based diol linker. Materials are synthesized following green chemistry principles using a direct acetoacetylation process of lignin in non-toxic solvents, which can subsequently be used to produce homogeneous materials. The thermomechanical properties and recyclability over five cycles demonstrate that the materials represent a promising class of tougher, greener, and sustainable vitrimers. The stress-relaxation properties of the materials are characterized through a detailed study focusing on the influence of the glass transition temperature of the materials. Mechanical testing yielded elastic moduli of up to 0.83 GPa and tensile strengths of up to 30 MPa. Additionally, processing through injection molding was demonstrated, producing homogeneous samples for tensile testing.

Received 30th March 2025
Accepted 17th July 2025

DOI: 10.1039/d5ta02533h

rsc.li/materials-a

Introduction

New polymeric materials must possess a lot of characteristics to meet the societal demand for more sustainable options.[1] Recyclable bioplastics can enhance the sustainability of the commercial plastic life cycle as part of a circular economy, particularly when they adhere to green chemistry principles.[2,3] Macromolecules derived from biomass, such as starch, cellulose, mycelium, and lignin from lignocellulosic biomass, are favorable feedstocks for the design of new, more sustainable multifunctional polymers.[4–8] Lignin is derived as a primary component of plant biomass and, along with cellulose and hemicellulose, forms lignocellulosic biomass, which is the most abundant type of biomass on the planet.[9,10] Technical lignin is produced as a byproduct of different pretreatments or separation processes that use lignocellulosic biomasses as raw material, such as in pulp or second-generation ethanol production. The pulp mill remains the main commercial source of lignin.[11] While polysaccharides such as cellulose and hemicellulose are utilized in the production of bio-based compounds, lignin remains underutilized, despite its high potential as a substitute for the high demand of fossil-based raw materials.[2,3,12–14] Only 5% of the produced lignin is used in low-value applications, such as fillers, or is burned for energy and electricity.[15] The remaining lignin is either incinerated as a low-grade fuel or landfilled.[16] However, recent focus in academia and industry on the structure and valorization of lignin and its derivatives highlights their significant potential and interest for advanced applications.[15,17–19] In particular, lignin is used in composite materials, energy storage materials, as a starting material for small aromatic molecules such as vanillin, in lignin-based nanoparticles, and in active food packaging.[16,20–28] Currently, lignosulfonates account for 90% of the total commercial lignin market and approximately 1.8 million metric tons are produced annually.[29] Due to the presence of sulfonate groups, lignosulfonates are anionically charged and therefore water soluble.[30] This allows for the use of water-based solvent systems throughout the formation of lignosulfonate-based materials as potential alternatives for fossil-based products. For instance,

[a]Institute of Physical Chemistry, University of Hamburg, Grindelallee 117, 20146 Hamburg, Germany

[b]Institute of Membrane Research, Helmholtz-Zentrum Hereon, 21502 Geesthacht, Germany. E-mail: volker.abetz@hereon.de

† Electronic supplementary information (ESI) available. See DOI: https://doi.org/10.1039/d5ta02533h

these are used in applications such as animal feed, pesticides, surfactants, and plasticizers in concrete admixtures.[31–33]

Integrating the concepts or recyclability, renewability, and green chemical processes into the formation of polymer networks provides a framework for designing sustainable materials. The combination of natural bioresources, such as lignin, with the concept of dynamic covalent chemistry imparts mechanical reprocessing and recycling properties to the polymeric materials.[34] The concept of vitrimers was first introduced in 2011 by the group of Leibler, demonstrating materials with transesterification exchange reactions which were reprocessable *via* injection molding.[35] In most cases of vitrimers, the reprocessing is limited to compression molding. The group of Du Prez demonstrated extrusion and injection molding for vinylogous urethane (VU) vitrimers with low-viscosity.[36] Vitrimers become malleable and show a thermoplastic flow behaviour when exhibited to a certain stimulus, as they are dynamic associative networks which can rearrange their crosslinks at a constant crosslink density.[37] This phenomenon occurs through stimulus-activated exchange reactions (*e.g.*, temperature, solvent, light), in which inter-polymer bonds are simultaneously cleaved and reformed, thus combining the beneficial features of both thermosets and thermoplastics.[38] When the rate of exchange reactions becomes sufficiently fast, the viscosity of vitrimers is primarily controlled by these reactions, resulting in a decrease in viscosity. These characteristics enable for self-healing, recycling, injection molding, and an overall increased lifecylcle.[34] The valorization and utilization of lignin in vitrimer materials were investigated based through various associative dynamic covalent adaptable chemistries, including transesterification, transacetalization, transcarbomylation, imine bond exchange, transalkylation, and disulfide exchange.[39–44]

VU vitrimers are based on transamination dynamic covalent chemistry and do not require an external catalyst. Here, acetoacetylated monomers are crosslinked with an excess of amine linker molecules, allowing for molecular network rearrangements at elevated temperatures.[45] Krall *et al.* highlighted the potential of the multi-hydroxy building block of Kraft lignin monomers as precursors for vinylogous urethane vitrimers, as they can be easily acetoacetylated using *tert*-butyl acetoacetate (TBAA).[46] However, the first work incorporating lignin into the design of VU vitrimers was published in 2023 by Sougrati *et al.*, utilizing organosolv lignin. The organosolv lignin was modified in a mixture of poly(ethylene glycol) (PEG) using ethylene carbonate. After acetoacetylation, the mixtures were vitrified in chloroform ($CDCl_3$) through condensation with hexamethylenediamine, achieving a lignin content of 30–40 wt%. The different network structures exhibited glass transition temperatures (T_gs) from −28 to 18 °C.[47] Liu *et al.* focused on acetoacetylated purified alkali wheat straw lignin (Protobind 1000 by LignoPure), obtained through soda pulping, and utilized a bio-based fatty acid amine (Priamine™ 1075) to form fully bio-based vitrimer materials with a lignin content of 40–50 wt% for adhesive applications. The acetoacetylation was carried out in 1,4-dioxane (DOX) with TBAA, forming the vitrimers in 2-methyl tetrahydrofuran, with a T_g range of 87–134 °C and an *E* modulus of 184 MPa. The materials showed fast stress-relaxation (9 s at 180 °C) using a single Maxwell model to fit the stress-relaxation.[48] Recently, Sougrati *et al.* prepared VU lignin vitrimers from organosolv lignin with 20–50 wt% lignin, synthesizing the acetoacetylated lignin with 2,2,6-trimethyl-4*H*-1,3-dioxin-4-on (TMDO). The vitrimers were formed in $CDCl_3$ and could be chemically recycled in an acidic solution. They obtained *E* moduli of up to 71 MPa and stresses at break of up to 3.8 MPa.[49]

In this work, we present the synthesis and characterization of bio-based recyclable vinylogous urethane lignin vitrimers synthesized *via* direct acetoacetylation with TBAA, utilizing lignosulfonate (Ls) from native biomass without further purification. Additionally, to compare the influence of impurities and structure of large-scale technical Ls to the material, Lignova™ Crude (LnC) and Lignova™ Pure (LnC) from Fibenol OÜ derived from a mild enzymatic hydrolysis process were used to prepare materials. The acetoacetylated lignin molecules are combined with bio-based Priamine™ 1073 linkers. An acetoacetylated bio-based poly(oxy-1,3-propanediyl) (PPD) was used as a linear linker. We present synthetic procedures without the use of toxic solvents such as DOX, enabling the formation of lignin-based vitrimers in a non-toxic mixture of water/acetone. To the best of our knowledge, this is the first study on acetoacetylated technical lignin derived from the sulfite process and enzymatic lignin sources, conducted with the substitution of toxic solvents. The content of lignin was between 40–62 wt% and the VU chemistry enables fast processing *via* heat compression at 180 °C for 30 min with a pressure of 1.9–2.5 MPa. Furthermore, we present an in-depth characterization of the stress-relaxation behavior of the materials *via* a stretched exponential fit using the Kohlrausch–Williams–Watts (KWW) function for lignin-based VU vitrimers, demonstrating the influence of the chemical microstructure of the vitrimers and the T_g influence of both the linkers and the lignin molecules.[50] The described processes and materials will be useful as recyclable damping materials, coatings, or containers that provide protection against environmental stress while offering a closed carbon-cycle and industrial processing methods, such as injection molding.

Experimental

Materials

Acetone (technical grade, BCD Chemie GmbH), *tert*-butyl acetoacetate (TBAA, TCI, 98%), calcium chloride ($CaCl_2$, anhydrous, Merck KGaA, 100%), calcium hydride (Merck KGaA, 100%), chloroform-d_1 ($CDCl_3$, Deutero GmbH, 99.8%), dimethyl sulfoxide (DMSO, Merck, 99%), dimethyl sulfoxide-d_6 (DMSO-d_6, Deutero GmbH, 99.8%), *N*,*N*-dimethylformamide (DMF, VWR, 99.5%), *N*,*N*-dimethylformamide-d_7 (DMF-d_7, Deutero GmbH, 99.5%), *endo*-*N*-hydroxy-5-norbonene-2,3-dicarboxylic acid imide (NHND, Alfa Aesar, 97%), lignosulfonate (Ls, dealkaline sodium lignosulfonate L0045, prepared from needle-leaved trees and broad-leaved trees through treatment of sodium sulfite, TCI), Lignova™ Crude (LnC, prepared from hard-wood by mild thermo-mechanical pre-treatment process with enzymatic hydrolysis, Fibenol OÜ), Lignova™ Pure (LnP,

prepared from hard-wood by mild thermo-mechanical pre-treatment process with enzymatic hydrolysis, Fibenol OÜ), phosphorus trichloride (Fisher Scientific, 99%), pinacol (TCI, >98%), bio-based poly(oxy-1,3-propanediyl) (M_n = 400–600 g mol^{-1}, PPD, Sigma-Aldrich), Priamine™ 1073 (Priamine, M = 534.59 g mol^{-1}, Croda), tetrahydrofuran (THF, Fisher Scientific, 99.5%), tris(acetylacetonato)chromium(III) ($Cr(acac)_3$, Fisher Scientific) were purchased and used as received. The crude, brownish 2,2,6-trimethyl-4*H*-1,3-dioxin-4-one (TMDO, Sigma-Aldrich, >93%) was purified by vacuum distillation prior to use to obtain a pure colorless liquid. Triethylamine (Grüssing) was pre-dried over molecular sieves (4 Å) for 4 days. Then, calcium hydride was added and the white suspension was refluxed for 24 h. Anhydrous triethylamine was obtained by distillation and stored under inert gas over molecular sieves. *N*,*N*-dimethylformamide (anhydrous, DMF, Fisher Scientific, 99.8%), pyridine (anhydrous, Fischer Scientific, 99.8%), and *n*-pentane (anhydrous, Thermo Scientific, >99.5%) were stored over molecular sieves (4 Å) and under inert gas atmosphere. The NMR solvent mixtures DMF/DMF-d_7 and $CDCl_3$/pyridine were stored over molecular sieves (4 Å) to remove residual moisture.

Instrumentation

Nuclear magnetic resonance spectroscopy (^{1}H NMR, ^{13}C NMR, heteronuclear single quantum correlation spectroscopy (HSQC), and heteronuclear multiple bond correlation spectroscopy (HMBC)). Nuclear magnetic resonance spectroscopy (^{1}H NMR, ^{13}C NMR, heteronuclear single quantum correlation spectroscopy (HSQC), and heteronuclear multiple bond correlation spectroscopy (HMBC)) were performed on a Bruker Avance III HD (600 MHz or 400 MHz) and a Bruker Avance I (500 MHz) spectrometer (Bruker Corporation, Billerica, United States) with $CDCl_3$ or DMSO-d_6 as solvent. Sample concentrations were between 10–60 mg mL^{-1}, and measurements were recorded at 298 K. When needed for quantification, DMF was added as internal standard. Data processing was carried out with MestReNova (14.1.0, Mestrelab Research S.L, Santiago de Compostela, Spain).

^{31}P NMR spectra. ^{31}P NMR spectra were recorded according to a quantitative ^{31}P NMR protocol with a frequency of 243 MHz, 256 scans, an inverse gated decoupling pulse (zigig), a spectral width of 100 ppm, an acquisition time of 2.6913 s, a relaxation delay D1 of 10 s, and the center of spectrum at 140 ppm. As the solubility of the different lignin types varied, two different anhydrous solvent systems, DMF-d_7/DMF/pyridine or $CDCl_3$/pyridine were used as solvent.[51,52] Lignova™ Crude and Lignova™ Pure were dissolved in $CDCl_3$/pyridine and lignosulfonate was dissolved in DMF-d_7/DMF/pyridine. Prior to each measurement, all samples were stored at 50 °C under vacuum for at least 24 h and subsequently in a glass desiccator over anhydrous calcium chloride. For measurements in DMF-d_7/DMF/pyridine, 30 mg of lignin were dissolved in 338 μL of a mixture of DMF-d_7 and DMF (1 : 1, v/v). An amount of 75 μL of an internal standard solution of NHND in anhydrous DMF (18 mg mL^{-1}) and 75 μL of a relaxation agent solution of $Cr(acac)_3$ in anhydrous pyridine (5.7 mg mL^{-1}) were added under stirring. Afterwards the solution was stirred for 12 h. The reactive compound 2-chloro-4,4,5,5-tetramethyl-1,3,2-dioxaphospholane (ClTMDP, 75 μL) was added 15 min before analysis and left to react for 5 min while stirring.[53] For analysis, the mixture was transferred into an NMR-tube. The signal of phosphitylated NHND at 152.78 ppm was used as internal standard. For measurements in $CDCl_3$/pyridine, an amount of 30 mg lignin was dissolved in 500 μL of a mixture of anhydrous pyridine and $CDCl_3$ (1.6 : 1, v/v) under stirring. An amount of 100 μL of an internal standard solution (anhydrous pyridine and $CDCl_3$ (1.6 : 1, v/v)) containing 18 mg mL^{-1} NHND and 5 mg mL^{-1} $Cr(acac)_3$ was added and the obtained mixture was stirred for 12 h. The reactive compound ClTMDP (75 μL) was added 15 min before analysis and left to react for 5 min while stirring. For analysis, the mixture was transferred into an NMR-tube. The signal of TMDP + H_2O at 132.20 ppm was used as internal standard. Data processing was carried out with MestReNova (14.1.0, Mestrelab Research S.L, Santiago de Compostela, Spain).

Electrospray ionization (ESI). Electrospray ionization (ESI) was measured by a Bruker maXis ESI-Q-TOF device (Bruker Corporation, Billerica, United States) coupled with Dionex Ultimate 3000 UPCL (Dionex Corporation, Sunnyvale, United States) and direct injection. Data processing was carried out with MestReNova (14.1.0, Mestrelab Research S.L, Santiago de Compostela, Spain).

Attenuated total reflection-Fourier transformation-infrared (ATR FT-IR). Attenuated Total Reflection-Fourier Transformation-Infrared (ATR FT-IR) were measured in the range of 4400–600 cm^{-1} with a resolution of 4 cm^{-1} and 64 scans using a Bruker FT-IR Vertex 70 spectrometer (Bruker Optics GmbH & Co. KG, Ettlingen, Germany). Measurements and data processing were carried out with Opus (8.7, Bruker Optics GmbH & Co. KG, Ettlingen, Germany).

Elemental analysis (CHNSO). Elemental analysis (CHNSO) was performed on a Unicube analyzer (Elementar Analysensysteme GmbH, Langenselbold, Germany). Each analysis was carried out twice.

Grinding. Grinding of materials was performed using a Mixer Mill MM 400 (RETSCH GmbH, Haan, Germany) with steel screw-top jars and a steel grinding ball under horizontal oscillation. For cryogenic grinding, the loaded steel jar was cooled in liquid nitrogen for 15 min with subsequent grinding. Exact parameters are listed in Table S1, ESI.†

Heat compression. Heat compression was carried out with a 2-column lab press PW 10 with a heating plate system HKP 500 160 × 160 mm and a TRG 3 temperature control unit (Paul-Otto Weber GmbH, Remshalden, Germany). The lignin-based vitrimers were filled into a custom-built stainless-steel compression mold (circular geometry, d = 5 cm, Fig. S1, ESI†). The samples were heated for 5 min before pressing. Heat compression was performed to produce homogeneous bubble-free black polymer sheets. Exact parameters are listed in Table S1, ESI.†

Solubility and swelling tests. Solubility and swelling tests were performed by addition of 1 mL of solvent (deionized water, acetone) to approximately 50 mg of the respective sample in

a glass vial. The vials were subsequently sealed for 24 h and stored at 25 °C. Afterwards, the supernatant was decanted, and the sample was weighed and stored at 80 °C under reduced pressure for at least 24 h until a constant mass was measured.

Thermogravimetric analysis (TGA). Thermogravimetric analysis (TGA) was carried out on a TG 209 F1 Libra (NETZSCH Gerätebau GmbH, Selb, Germany) to determine the mass loss during heat treatment. A temperature range of 25–700 °C with a heating rate of 10 K min^{-1} under ambient atmosphere (oxygen) was used in a flow rate of 20 mL min^{-1}. Isothermal measurements were carried out at 180 °C for 3 h with ambient (oxygen) atmosphere in a flow rate of 20 mL min^{-1}. An amount of 10–15 mg was weighed into an aluminum crucible. Data processing was performed with Proteus Analysis (8.0.3, NETZSCH-Gerätebau GmbH, Selb, Germany).

Differential scanning calorimetry (DSC). Differential scanning calorimetry (DSC) was carried out on a 204 F1 Phoenix (NETZSCH Gerätebau GmbH, Selb, Germany) to determine the thermal properties of the lignins and lignin-based materials. An amount of 5–10 mg was weighed into an aluminum crucible. The heating rate was set to 10 K min^{-1} or 20 K min^{-1} using a nitrogen atmosphere with a flow rate of 20 mL min^{-1}. A temperature range between −50–200 °C or −80–250 °C was used in three heating cycles. The thermal properties were analyzed determining using the DSC data of the second heating curve. Data processing was performed with Proteus Analysis (8.0.3, NETZSCH-Gerätebau GmbH, Selb, Germany).

Optical microscopy (OM). Optical microscopy (OM) images were taken with a Keyence VHX-6000 digital microscope with a VH-Z20UR lens (Keyence Deutschland GmbH, Neu-Isenburg, Germany).

Scanning electron microscopy (SEM). Scanning electron microscopy (SEM) images were recorded on a LEO Gemini 1550 (Carl Zeiss, Oberkochen, Germany). Secondary electrons were detected with an Everhart-Thornley detector, operating with 1–5 kV and 50–100 pA.

Dynamic light scattering (DLS). Dynamic light scattering (DLS) analysis was carried out using an ALV/LSE-5003 multi-tau digital correlator and a He–Ne laser (633 nm, 35 mW) using a measurement angle of 90° and a duration of 30 s. Three measurements were performed for each sample and the mean value was calculated. The temperature was set to 30 °C with a toluene bath. The data was analyzed using a MATLAB R2021a script written by B. Hankiewicz. The hydrodynamic radius R_h was calculated assuming spherical particle geometry starting at a minimum radius of 5 nm. The solutions for the measurement were prepared dissolving the analyte with a concentration of 3 mg mL^{-1} in a mixture of acetone/water (9 : 1, v/v) or DMSO.

Atomic force microscopy (AFM). Atomic force microscopy (AFM) investigations of the vitrimer films were performed in intermittent contact mode using a JPK Nanowizard (Bruker Corporation, Billerica, United States of America) microscope with a Si-tip ($f = 280$ kHz, $r = 10$ nm).

Energy-dispersive X-ray spectroscopy (EDX). Energy-dispersive X-ray spectroscopy (EDX) was carried out using the SEM LEO Gemini 1550 (Carl Zeiss, Oberkochen, Germany) with its adjunct EDX analyzer Ultim Max 100 Silizium Drift Detector (Oxford Instruments, High Wycombe, United Kingdom).

Stress–strain measurements. Stress–strain measurements were performed at room temperature ($T = 23$ °C) on a universal testing machine zwickiLine Z 5.0 TH (ZwickRoell GmbH & Co. KG, Ulm, Germany) using a 5 kN load cell. The measurements were carried out in accordance with the test standard DIN EN ISO 527-1. The initial force was set to 0.1 MPa, and the clamping length was 13.24 mm. The elastic modulus was determined at a speed of 1 mm min^{-1} and the rest of the test was carried out at 10 mm min^{-1}. Data was processed using TestXpert II (3.71, ZwickRoell GmbH & Co. KG, Ulm, Germany). Test specimens were punched out with a cutting press type ZCP020 (ZwickRoell GmbH & Co. KG, Ulm, Germany) with the attachment for test specimens of type 5 B (according to DIN EN ISO 527-2-5B). Durability tests were performed in an oscillating procedure, with a speed of 1 mm min^{-1} until a force of 50 N was reached. The initial force was set to 0.05 N, and the clamping length was 5 mm. Afterwards, the stress was released until a force of 0.1 N was reached. 1000 consecutive cycles were performed on a test specimen with the dimensions 10 × 10 × 1 mm.

Dynamic-mechanical analysis (DMA). Dynamic-mechanical analysis (DMA) was carried out with an Anton Paar MCR 502 rheometer (Anton Paar GmbH, Graz, Austria) using a plate–plate geometry with a diameter of 8 mm. The measurements were carried out using a heat chamber (Anton Paar CTD180) with a nitrogen atmosphere, a Peltier plate temperature control and a normal force of 1 N. The gap between the upper and the lower plate was usually set to 1 mm and each sample was annealed for at least 3 min before starting the respective measurement. Prior to all rheological measurements, amplitude sweeps between 0.001% and 10% shear strain γ were performed at a constant angular frequency of 6.28 rad s^{-1} at 110 °C. This should ensure that the chosen strain amplitude γ_0 is located within the linear viscoelastic regime of the material, so that the storage modulus G' and the loss modulus G'' were independent of strain. Temperature-sweep measurements were carried out in oscillatory mode with a constant angular frequency of 6.28 rad s^{-1} at a constant shear strain of 0.01% in the temperature range of 150–0 °C at a rate of 2 K min^{-1}. Stress relaxation measurements were carried out with a shear strain of 1% at temperatures in the range of 180–110 °C. Data processing was performed with RheoCompass (1.32, Anton Paar GmbH, Graz, Austria). Specimens for the DMA were punched out with an 8 mm tool.

UV-light irradiation testing. UV-light irradiation testing was performed using an OmniCure® AC 450 UV lamp (Polytec GmbH, Waldbronn, Germany) with a wavelength of 365 nm and an optical power of 45 W. A GTC 400 C Professional thermal imaging camera (Robert Bosch Power Tools GmbH, Leinfelden-Echterdingen, Germany) with a 19 200-pixel infrared sensor was used to capture images after 10 s, 60 s, and 300 s of irradiation.

Injection molding. Injection molding was carried out using a MiniJet Pro (Thermo Fisher Scientific, Waltham, United States) with a melt temperature of 250 °C, a mold temperature of 220 °C, and an injection pressure of 1000 bar. A typical injection molding protocol was carried out as follows: the

ground sample was heated for 5 min. Then, the injection pressure was applied for 45 s with a subsequent rest time of 20 s at 100 bar using a mold for tensile test specimens DIN EN ISO 527-2-5B or a rectangular mold of the size 10 × 10 × 4 mm.

Shore hardness. Shore hardness was measured using a Manual Shore test stand TI-AC with an analogue Shore hardness tester HBA 100-0 (Kern & Sohn GmbH, Baldingen-Frommern, Germany) and a Manual Shore test stand TI-D with an analogue Shore hardness tester HBD 100-0 (Kern & Sohn GmbH, Baldingen-Frommern, Germany). The Shore-Hardness was determined according to DIN ISO 7619-1 using a material block formed by injection molding of a size of 10 × 10 × 4 mm and a time of 15 s, before the hardness was measured. An average of five measurements was used to calculate the hardness according to the Shore D scale.

Synthetic procedures

Acetoacetylation of lignosulfonate (Ls). Lignosulfonate (30.45 g) was dissolved in DMSO (90 mL) at 80 °C under stirring until a homogeneous dark brown mixture was obtained. Afterwards, TBAA (58 mL) was added and the mixture was heated to 135 °C for 6 h, while the byproduct *tert*-butanol was removed by distillation during the reaction. The solvent was removed under reduced pressure at 135 °C until a black solid was obtained. Subsequently, the obtained solid was ground into a brown powder and further dried under vacuum at 60 °C for at least 15 h. The dried product was stored in a glass desiccator over $CaCl_2$.

Acetoacetylation of Lignova™ Crude (LnC). Lignova™ Crude (20.08 g) was dissolved in DMSO (120 mL) at 120 °C under stirring until a homogeneous dark brown mixture was obtained. Afterwards, TBAA (33 mL) was added and the mixture was heated to 135 °C for 6 h, while the byproduct *tert*-butanol was removed by distillation during the reaction. The solvent was removed under reduced pressure at 135 °C until a black solid was obtained. Subsequently, the obtained solid was ground into a brown powder and dried under vacuum at 60 °C for at least 15 h. The dried product was stored in a glass desiccator over $CaCl_2$.

Acetoacetylation of Lignova™ Pure (LnP). Lignova™ Pure (20.13 g) was dissolved in DMSO (70 mL) at 80 °C under stirring until a homogeneous dark brown mixture was obtained. Afterwards, TBAA (43 mL) was added and the mixture was heated to 135 °C for 6 h, while the byproduct *tert*-butanol was removed by distillation during the reaction. The solvent was removed under reduced pressure at 135 °C until a black solid was obtained. Subsequently, the obtained solid was ground into a brown powder and dried under vacuum at 60 °C for at least 15 h. The dried product was stored in a glass desiccator over $CaCl_2$.

Acetoacetylation of bio-based poly(oxy-1,3-propanediyl) (PPD). The synthesis was performed according to a standard procedure for the acetoacetylation of hydroxy groups.[54] TMDO (38 mL) and PPD (50.11 g) were mixed *via* stirring at room temperature. After a homogeneous solution was obtained, the mixture was heated to 135 °C under stirring. The byproduct acetone, dehydroacetic acid and residual TMDO were removed by distillation. The mixture was dried in vacuum at 135 °C to give acetoacetylated PPD (APPD) as a dark red liquid (6.90 g, 97%).

Vitrimer formation in water/acetone. The formation of vitrimers was performed in a mixture of water and acetone (1 : 4, v/v) to ensure a sustainable and environmentally friendly route. Exact parameters are listed in Table S1, ESI.† An exemplary synthesis was conducted as follows: Acetoacetylated lignin was dissolved in 10 mL of the solvent mixture at ambient temperature (23 °C) under stirring until a homogeneous black mixture was obtained, which usually took 60 min. If APPD was used, it was added together with the lignin. Subsequently, the amine linker Priamine™ 1073 was added while vigorously stirring. The mixture was left to react for 30 min without stirring. Then, the black gel-like mixture was carefully heated step-wise up to 120 °C while stirring. The black solid was dried under reduced pressure at 100 °C for at least 13 h and subsequently at 150 °C for 1 h. The obtained black material was ground with a ball mill into a brownish powder. A film of 1 mm thickness was pressed using heat compression in a custom-made stainless-steel mold with a diameter of 5 cm (Fig. S1, ESI†).

Results and discussion

Acetoacetylation of lignosulfonates and enzymatic lignin

The variety and complexity of lignin's structure and functional groups are advantageous for many applications. However, underlying limitations such as poor solubility and barriers to traditional analytics have been addressed, thereby increasing the suitability of lignin in many chemical processes. Different lignin resources with different degrees of purity were tested to determine the applicability of the hereby developed procedure, with lignosulfonate (Ls) as an example of a large-scale industrial grade lignin containing impurities and sulfonate, and Lignova™ Crude (LnC) as well as Lignova™ Pure (LnP) as sulfur-free lignin alternatives with higher purity. Further information on the lignins can be found in Table 1.

To achieve a reliable and reproducible acetoacetylation, the hydroxy content of the raw lignins was first determined *via* quantitative ^{31}P NMR spectroscopy to calculate the necessary amount of acetoacetylation agent, *tert*-butyl acetoacetate (TBAA). This analytical protocol involves the phosphitylation of the hydroxy (OH) groups of a lignin sample followed by ^{31}P NMR spectroscopy.[51,52,55] Depending on the solubility of the different lignins, two different solvent systems were used, consisting either of $CDCl_3$ for LnP and LnC or DMF/DMF-d_7 for Ls. For the latter, phosphitylated aliphatic hydroxy groups appear in the range of 152.0–145.5 ppm, phosphitylated phenolic hydroxy groups between 145.5–137.5 ppm, and phosphitylated carboxylic groups between 137.5–135.0 ppm, respectively (Fig. S2–S4, ESI†).[52] The amount of hydroxy groups was determined using eqn (S1) (ESI†) and are listed Table 2. Since the acetoacetylation of carboxylic groups can produce reactive and easily hydrolysable carboxylic anhydrides, these groups were not considered in the following. For Ls, LnC, and LnP, total amounts of 2.69 mmol g^{-1}, 3.68 mmol g^{-1}, and 3.50 mmol g^{-1} of non-carboxylic OH groups were determined, respectively. These

Table 1 Comparison of the different lignin sources used in this work. Structures are just examples that represent common substructures and functional groups for the respective lignin-type

	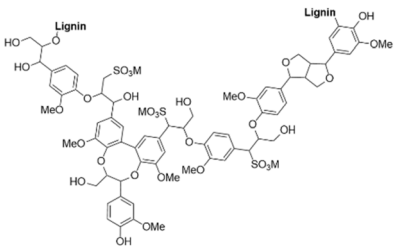	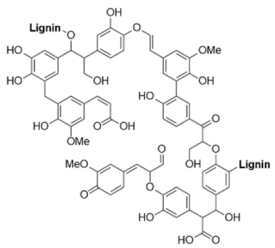
	Lignosulfonate (Ls)	Lignova™ Crude (LnC)[a]	Lignova™ Pure (LnP)[a]
Molar mass [Da]	1000–400 000 (ref. 56)	16 000 (average)	10 000 (average)
Sulfur content [%]	4.4[b]	<0.2	<0.2
Saccharide content [%]	—	<3	—
Solubility	Water/DMSO	Organic solvent	Organic solvent
Ash and ionic content [%]	18[c]	0.3	1.7

[a] Information was provided by Fibenol OÜ. [b] Determined by elemental analysis. [c] Determined by TGA displaying the amount of substance left after complete decomposition.

Table 2 Calculated amount of OH moieties from quantitative analysis of different lignins (Ls, LnC, and LnP), as well as of respective acetoacetylated species (ALs, ALnC, ALnP) by ^{31}P NMR and ^{1}H NMR spectroscopy. Conversion rates of acetoacetylated species are calculated based on the OH content determined by ^{31}P NMR for respective lignin resource

		OH content [mmol g^{-1}]		
Lignin		Aliphatic OH [mmol g^{-1}]	Phenolic OH [mmol g^{-1}]	Total non-carboxylic OH [mmol g^{-1}]
Ls		1.37	1.32	2.69
ALs		0.08	0.81	0.89
Conversion	^{31}P	94%	39%	67%
	^{1}H	—	—	61%
LnC		2.06	1.62	3.68
ALnC		0.04	1.01	1.05
Conversion	^{31}P	98%	38%	71%
	^{1}H	—	—	70%
LnP		1.51	1.99	3.50
ALnP		0.03	1.33	1.36
Conversion	^{31}P	98%	33%	61%
	^{1}H	—	—	65%

values may also include impurities, such as low molecular weight carbohydrates, which are included into the VU network, since the lignin sources were not further purified.

Especially LnC contains still remaining saccharides after the hydrolysis process which are responsible for the higher amount of aliphatic OH observed as sharp peaks in the aliphatic region of ^{31}P NMR spectroscopy.[57] The acetoacetylation of OH groups with TBAA is well known and involves the intermediate formation of reactive acetyl ketene by cleavage of TBAA under the release of *tert*-butanol, which can be removed by distillation throughout the reaction.[54] In this work, DMSO was used as an alternative solvent replacing carcinogenic DOX and DMF, which have been used for the direct acetoacetylation of lignin.[46,48] DMSO acts as a solvent and also prevents precipitation of the acetoacetylated products during the reaction.

In FT-IR, the acetoacetylated lignins present the characteristic peaks of acetoacetate bonds at around 1712 cm^{-1} and 1741 cm^{-1} (Fig. 1a). For ALs, the latter appears as a broad shoulder. The ^{1}H and ^{13}C NMR spectra are provided in the ESI, Fig. S5–S10.† A broad peak between 2.4 ppm and 1.8 ppm can be assigned to the terminal methyl group of acetoacetates (Fig. 1b).[46,49] 2D NMR techniques (HSQC and HMBC) were used to verify the signals from ^{1}H NMR (Fig. S11–S16, ESI†). The methylene group of acetoacetates can be assigned to a broad signal at 3.6 ppm, that undergoes ^{1}J coupling with the carbon atom of the methylene group at 50 ppm. Also, further characteristic ^{2}J couplings for acetoacetates can be observed *via* HMBC. Interestingly, ^{2}J coupling between the methylene group and carbonylic carbon atoms of acetoacetylated lignins can only be observed when measuring with 600 MHz, as seen in the 2D spectra of ALs, probably as a result of the low intensity of ^{13}C NMR. Quantification of acetoacetylation of ALs, ALnC, and ALnP was examined by ^{31}P NMR and ^{1}H NMR. As a result of the acetoacetylation of hydroxy moieties, the number of hydroxy groups decreases. The decreased amount of OH moieties observed in the ^{31}P NMR spectra can thus be assigned to acetoacetylated groups. Notable, this analytical procedure can distinguish the different conversions of aliphatic and phenolic hydroxy groups of lignins. A conversion of over 90% for aliphatic hydroxy groups and of 33–39% for aromatic hydroxy groups was calculated (Table 2), as it was also observed in the literature for similar model compounds.[46] The difference in conversions can be attributed to the accessibility of the aliphatic hydroxy groups and the slower rate of conversion for aromatic hydroxy groups. Additional broadened peaks between 135.0 ppm and 134.0 ppm can be assigned to the phosphitylated enol form of acetoacetates.[47] To simplify the analysis of

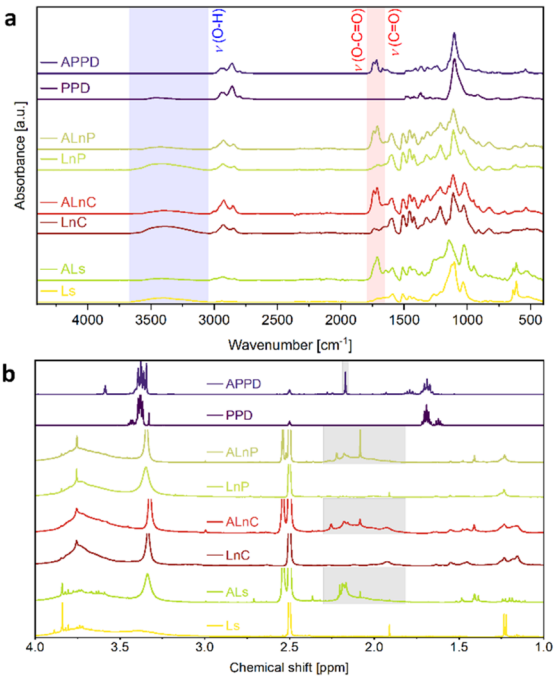

Fig. 1 (a) ATR-FT-IR spectra of the different lignin sources (Ls, LnC, and LnP), as well as of poly(oxy-1,3-propanediyl) (PPD) and the respective acetoacetylated species (ALs, ALnC, ALnP, and APPD) showing the characteristic bands of the acetoacetate group with the C=O ester (1735–1741 cm^{-1}) and C=O ketone (1712–1716 cm^{-1}) stretching vibration bands. The lignin backbone represents the C–O (995–1148 cm^{-1}), C–C (2850–3050 cm^{-1}), C=C (1148–1650 cm^{-1}), and O–H (3050–3650 cm^{-1}) stretching vibration bands. (b) ^{1}H NMR spectra of PPD, LnP, LnC, and Ls, as well as the acetoacetylated APPD, ALnP, ALnC, and ALs, showing the characteristic chemical shift of the acetoacetate groups (grey) (400 MHz, 298 K, DMSO-d_6).

acetoacetylated lignin sources, a ^{1}H NMR protocol was employed, using a known amount of DMF as an internal standard, allowing for direct calculation of acetoacetate moieties from the ^{1}H NMR (Fig. S17–S19, ESI†). Here, integrals of the proton of DMF appearing at 7.95 ppm and the broad peak between 2.4–1.8 ppm of the methylene group of the acetoacetate moieties was used to calculate the amount of acetoacetate moieties. Comparison between the results in Table 2 show the values from both NMR techniques in good agreement and only a maximum deviation of 6%. For this procedure, the highest amount of acetoacetate moieties was achieved with LnC because of the higher content of aliphatic hydroxy groups. Thus, the choice of lignin influences the acetoacetylation process and conversions can be calculated by quantitative NMR spectroscopy methods. For increasing the processability of the Ls-based vitrimers (*vide infra*), smaller molecules were added to the formulation of the materials. Therefore, bio-based poly(oxy-1,3-propanediyl) (PPD) (^{1}H NMR, ^{13}C NMR and ESI-MS spectra, Fig. S20–S22, ESI†) was used in an acetoacetylation protocol using TMDO. The successful acetoacetylation of acetoacetylated PPD (APPD) is proven by FT-IR, ^{1}H NMR, ^{13}C NMR, and 2D NMR spectroscopy (Fig. 1, H NMR, ^{13}C NMR, HSQC, and HMBC spectra are displayed in more detail in Fig. S23–S29, ESI†).

Synthesis and network formation of VU-based lignin vitrimers

Vitrimers from ALs, ALnC, and ALnP were synthesized in a mixture of acetone and water (4 : 1, v/v) by performing a condensation reaction with the amine functions of Priamine™ 1073 (Priamine), displayed in Scheme 1. A higher concentration of acetone reduces the solubility of acetoacetylated lignins, while an increased amount of water decreases solubility of Priamine. Therefore, a 4 : 1 (v/v) ratio of acetone to water was found as optimal for the formation of vinylogous urethanes, ensuring adequate solubility of all reactants. In the case of VU-(ALs/APPD$_x$-Pri)$_{0.6}$-Vitrimers, APPD was added to the mixture to ensure homogeneous materials. Especially for ALs-based systems, it was found that a higher content of lignin (>55 wt%) resulted in brittle materials, which were too brittle to be processed (Fig. S30, ESI†). By adding APPD as a plasticizer, homogeneous films can be produced and samples with three different weight percentages of APPD (5, 10, 15 wt%) were investigated. To minimize the factors of the amine-linker contributing to changes in material behavior and properties, the amount of amines was kept constant. This results in changing both the amount of lignin and APPD in the sample series. All vitrimer formulations are listed in Table S1, ESI† with the mass fractions of lignin, APPD, and amine building block listed in Table 3.

After a homogeneous mixture was obtained, Priamine was added, leading to gelation, which indicated a crosslinking reaction. Subsequently, the solvent and byproducts were removed, and the black residue was ground into a powder. This procedure ensures a homogeneous distribution of acetoacetylated lignin across the entire material. By using an excess of amine, the transamination reaction can be triggered by a thermal stimulus, which is the required dynamic exchange reaction for the vitrimer.[58] The excess of amines can be expressed by the *R*-value, which is the ratio of amine to acetoacetate functions. Here, *R*-values between 0.4–0.9 were chosen to ensure processability. The Ls-based vitrimers required a higher number of amines (*R*-values of 0.4–0.6) to produce processable materials, which may be attributed to the sulfonate moieties potentially deactivating amine groups. The formation of lignin-based VU vitrimers can be characterized by FT-IR spectroscopy with new absorption bands between 3000 cm^{-1} and 2850 cm^{-1}. Moreover, the characteristic acetoacetate bands at 1741 cm^{-1} and 1711 cm^{-1} are absent, indicating full conversion of the acetoacetate functions (Fig. S31–S34, ESI†).

To ensure that the grinding process before the vitrimer film formation has no influence on the backbone structure of the lignin vitrimer materials, FT-IR spectra were measured for all materials after the ball milling process and before sample formation, displayed in Fig. S35–S46.† The results indicate no change in the backbone structure with observable unreacted acetoacetate groups before heat compression. The heat compression process results in homogeneous films with all acetoacetates reacted after film formation due to the applied pressure and temperature. This behaviour is particularly evident for the materials VU-(ALnC-Pri)$_{0.7}$, Fig. S41,† VU-(ALnC-Pri)$_{0.9}$, Fig. S43,† and VU-(ALnP-Pri)$_{0.8}$, Fig. S45.†

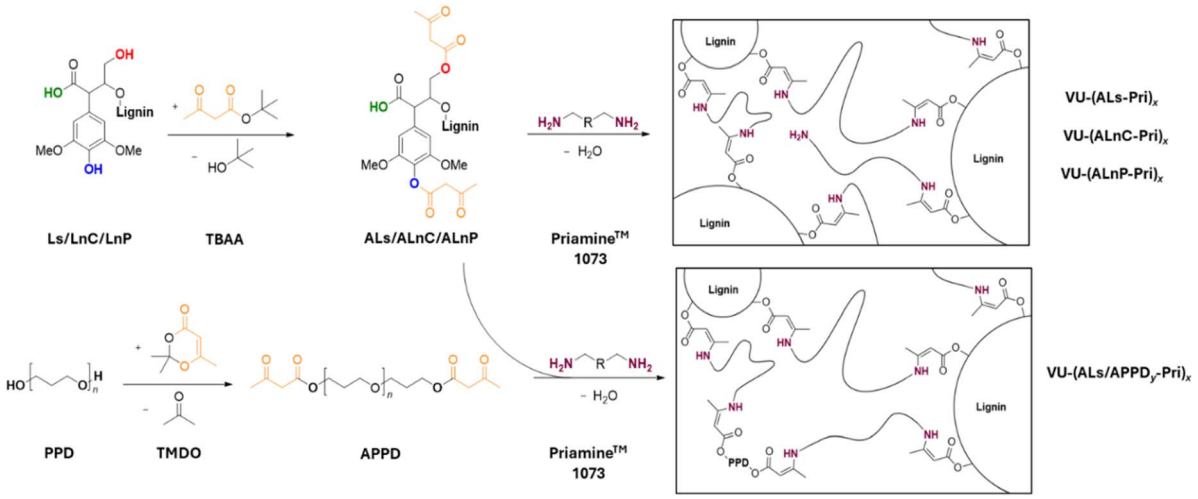

Scheme 1 Synthesis of acetoacetylated lignins (ALs, ALnC, and ALnP) from the different lignin sources (Ls, LnC, and LnP) with *tert*-butyl acetoacetate (TBAA) and acetoacetylated APPD from PPD using 2,2,6-trimethyl-1-3-dioxin-4-one (TMDO). Subsequently, the formation of vinylogous urethane vitrimers through a condensation reaction with Priamine™ 1073 gives the polymer materials VU-(ALs-Pri)$_x$, VU-(ALnC-Pri)$_x$, VU-(ALnP-Pri)$_x$, and VU-(ALs/APPD$_y$-Pri)$_x$, with x abbreviating the R-value and y abbreviating the amount [wt%] of APPD in the formulations.

Swelling tests were performed to confirm the network structure by exposing the polymeric materials to water and acetone. The swelling ratio (S) and the soluble fraction (SF) were calculated with eqn (S2) and (S3),† results are listed in Table S2, ESI.† Maximum values of S at 41% indicate network formation, while SF-values of less than 10% demonstrate the integrity during the swelling and confirm the reaction of acetoacetates and amines to form vinylogous urethanes. Interestingly, LnC- and LnP-based vitrimers exhibited almost no swelling (1.6–5.1%) and negligible soluble fraction values (≤0.3%) in water. The sulfonate groups and their corresponding ionic structures in the LS vitrimers results in higher values for S and SF, reaching up to 39% and 4.4%, respectively, in water. In acetone, higher values for S of up to 36% and for SF of up to 9.6% were observed. Notably, technical lignin sources can contain impurities such as ash, inorganic salts and compounds of low molecular weight compounds, which can lead to an increase in SF. All in all, the vitrimers from Ls, LnC, and LnP demonstrate intact network structures. Furthermore, the results indicate that impurities can influence the swelling properties.

Analysis of the morphology

Optical microscopy (OM) was performed on the raw lignin samples and the acetoacetylated lignins to evaluate the morphology of the vitrimer materials. The lignin precursors were ground in a ball mill to achieve a homogeneous structure and to break down aggregates. The OM images indicate that there are no significant visible differences in the lignins before and after the modification (Fig. S47, ESI†).

In SEM, the lignin sources display a particle-like structure with aggregated lignin fragments (Fig. S48–S50, ESI†). The structures of the agglomerated fragments appear smaller for

Table 3 Overview of the composition of the different vitrimer materials with details of the respective lignin source, the lignin content, the APPD content, the Priamine™ 1073 content and the R-value

Sample	Lignin content [wt%]			APPD [wt%]	Priamine [wt%]	R-value [—]
VU-(Lignin/APPD-Pri)$_x$	ALs	ALnC	ALnP	APPD	Pri	x
VU-(ALs-Pri)$_{0.4}$	46	—	—	—	54	0.4
VU-(ALs-Pri)$_{0.5}$	50	—	—	—	50	0.5
VU-(ALs-Pri)$_{0.6}$	54	—	—	—	46	0.6
VU-(ALs/APPD$_5$-Pri)$_{0.6}$	51	—	—	5	44	0.6
VU-(ALs/APPD$_{10}$-Pri)$_{0.6}$	46	—	—	10	44	0.6
VU-(ALs/APPD$_{15}$-Pri)$_{0.6}$	41	—	—	15	44	0.6
VU-(ALnC-Pri)$_{0.7}$	—	50	—	—	50	0.7
VU-(ALnC-Pri)$_{0.8}$	—	53	—	—	47	0.8
VU-(ALnC-Pri)$_{0.9}$	—	57	—	—	43	0.9
VU-(ALnP-Pri)$_{0.7}$	—	—	55	—	45	0.7
VU-(ALnP-Pri)$_{0.8}$	—	—	59	—	41	0.8
VU-(ALnP-Pri)$_{0.9}$	—	—	62	—	38	0.9

LnC and LnP than for Ls, which can also be assumed by comparison of the molecular mass distribution in Table 1. These aggregates could result from intrinsic self-assembly of lignin organic moieties and their amphiphilic properties, especially found in lignosulfonates.[27] To verify the existence of particles, acetoacetylated lignin species ALs and ALnP were dissolved in acetone/water (9 : 1, v/v) or DMSO and dynamic light scattering (DLS) was performed on the solutions. ALnC was not examined *via* DLS because the samples did not fully dissolve in the solvent systems. For ALs and ALnP, hydrodynamic radii of approximately 90 nm and 50 nm were found, respectively with a narrower distribution for ALnP (Fig. S51, ESI†). These hydrodynamic radii are in a similar range found for lignin nanoparticles, ranging between 50–176 nm.[27,59,60] It is important to note that the observed small reduction in the correlation curve at 10^{-3} ms of ALnP could indicate the presence of smaller species which could not be resolved in the size distribution.

In order to investigate the morphology of the lignin vitrimer films, they were also examined using the SEM. Fiber-like structures appear in the cross-section for ALs-based vitrimers VU-(ALs-Pri)$_{0.5}$ (Fig. S52, ESI†) and VU-(ALs/APPD$_{10}$-Pri)$_{0.6}$ (Fig. S53, ESI†). These fragments were further characterized using energy-dispersive X-ray spectroscopy (EDX), measuring a high amount of sodium, oxygen, and sulfur in these structures. An EDX spectrum next to the fragments only obtained carbon and oxygen (Tables S3 and S4, ESI†). In contrast, the vitrimer films based on enzymatic lignin exhibit a homogeneous internal structure with no visible lignin fragments in the SEM images (Fig. S54 and S55†). This is similar to what has been observed in other homogeneous lignin systems based on Kraft lignin or organosolv lignin.[61] The higher homogeneity of the material could also be caused by the smaller particle size distribution of ALnP compared to ALs, as can be seen in DLS. This can then lead to a better distribution of lignin moieties and therefore, a more homogeneous material. Additional EDX measurements for ALnC and ALnP based materials VU-(ALnC-Pri)$_{0.8}$ and VU-(ALnP-Pri)$_{0.8}$ are presented in Tables S5 and S6, ESI.† The results show that no sulfur or sodium is present, which is in good agreement with the purity of the enzymatic lignins.

A difference in the morphology can be observed in AFM height images of the vitrimer films. AFM images showing both height and phase information are displayed in Fig. S56–S59, ESI.† The surface plot of VU-(ALs-Pri)$_{0.5}$ shows a rough surface with a homogeneous distribution of lignin fragments. For VU-(ALs/APPD$_{10}$-Pri)$_{0.6}$, a more regular surface is observed, indicating an influence of APPD and a lower mass fraction of lignin. Both AFM images of VU-(ALnC-Pri)$_{0.8}$ and VU-(ALnP-Pri)$_{0.8}$ display surface morphologies with smaller granules and less irregularities. The surface structure is most likely caused by the polytetrafluorethylene (PTFE) sheets used for heat compression.

Despite the existence of particles observed by DLS, no particle-like structure could be detected in the material by SEM and AFM, confirming a homogeneous formation of lignin-based vitrimers.

Thermomechanical properties

To determine the thermomechanical stability of the lignin vitrimers, thermogravimetric analysis (TGA) was conducted on each prepared material under ambient (oxygen) atmosphere (Fig. S60, ESI†). The decomposition temperature $T_{5\%}$, defined as the temperature at which 5% mass loss of the initial sample occurs, ranged from 272–307 °C, indicating that all samples exhibited good thermal stability. This $T_{5\%}$ range was also observed for VU vitrimers produced from oxyalkylated acetoacetylated organosolv lignin (OOSL, 266 °C), organosolv lignin (OSL, 270 °C), and for soda pulped wheat straw lignin (WSL) (309 °C).[47–49] The residual weight of the Ls-based films of 15–23% is attributed to carbonized material (char) and ionic residues. To ensure thermal stability during heat compression, isothermal TGA was conducted for 3 hours at 180 °C under ambient (oxygen) atmosphere (Fig. S61, ESI†). All samples exhibited an isothermal mass loss of 1–3%, indicating stability under the processing conditions during dynamic mechanical analysis, heat compression, recycling, and stress relaxation measurements.

Thermal properties were further analyzed using dynamic differential scanning calorimetry (DSC). The measured heat flow was represented by a flat curve without significant transitions (Fig. S62, ESI†). A clear glass transition could not be detected in the samples; instead a broad glass transition region was observed between −50–250 °C, with a slight shift to higher temperatures when using ALnC and ALnP as a monomer. These glass transition regions can be attributed to the distribution of acetoacetylated lignin within the polymeric APPD and Priamine chains, which broadens the glass transition range.[56] This observation can also be verified by DMA, which found a tan(δ) with a broad distribution for ALs-based materials and distinguishable glass transitions for ALnC- and ALnP-based materials.

Mechanical properties

The mechanical properties of the lignin vitrimers were determined through uniaxial tensile testing at room temperature (23 °C). Stress–strain curves of the materials are presented in Fig. 2. The strength and strain behavior of the materials are influenced by the type of lignin used in the formulation, the lignin content, the APPD content, and the *R*-value. The materials range from softer films to more rigid structures, exhibiting averaged elastic moduli (E) from 108 MPa to 837 MPa, tensile strengths (σ_m) from 6.0 MPa to 30.3 MPa, and elongations at strain at break (ε_m) ranging from 2.1% to 20.1%. The results indicate that as the *R*-value increases, the values of E also increase, resulting in more rigid materials, as demonstrated by the decreasing values of ε_m. On one hand, this is attributed to the decreasing number of dangling amine groups in the materials. On the other hand, the relative amount of lignin crosslinker increases with higher *R*-values, highlighting the influence of the rigid lignin molecules. The mixtures and results are displayed in Fig. 3 and listed in Table S7.† In case of the lignosulfonate materials, σ_m increases from 13.5 ± 0.2 MPa for VU-(ALs-Pri)$_{0.4}$ to 17.5 ± 1.3 MPa for VU-(ALs-Pri)$_{0.5}$. However, this trend is not continued

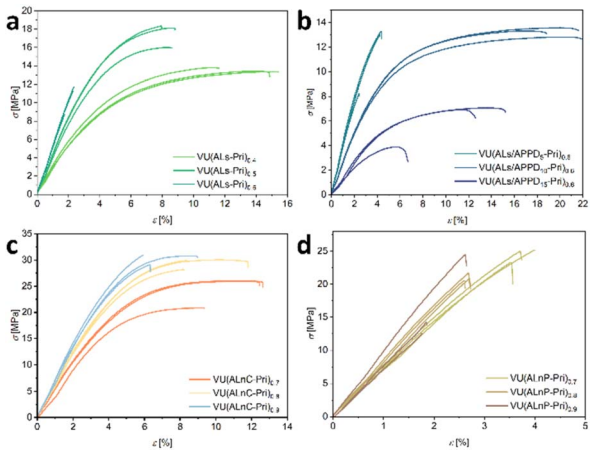

Fig. 2 Stress–strain curves (T = 23 °C) of the lignin vitrimer materials derived from ALs (a and b), ALnC (c), and ALnP (d). The materials range from softer films to more rigid ones, showing averaged elastic moduli (E) in the range of 108 MPa up to 837 MPa, tensile strengths (σ_m) of 6.0 MPa up to 30.3 MPa, and elongations at an ultimate stress (ε_m) of 2.1% to 20.1%.

for VU-(ALs-Pri)$_{0.6}$, as the material becomes brittle, as displayed by the low value of ε_m (2.1% ± 0.3%). To ensure good processability and reduce brittleness, a linear APPD crosslinker was introduced at concentrations of 5 wt%, 10 wt%, and 15 wt% while maintaining a constant R-value (Fig. 2b and 3b, c). As expected, with increasing amounts of APPD, ε_m increases, with material VU-(ALs/APPD$_{10}$-Pri)$_{0.6}$ exhibiting the best compromise between strength and toughness, showing σ_m values of 13.0 ± 0.3 MPa and ε_m values of 20.1% ± 1.7% for an R-value of 0.6. This demonstrates the potential to modify the materials not only by varying the amount of free amines, but also by compounding with shorter, flexible molecules in a straightforward manner to prepare materials with desired properties. Overall, the vitrimers prepared from enzymatic lignin exhibit higher values of E and σ_m compared to those based on lignosulfonate, highlighting the influence of the morphology and fewer impurities in the crosslinking compound. Additionally, there are increasing values of E and σ_m associated with higher R-values (Fig. 3b and c). The highest value of σ_m was observed for VU-(ALnC-Pri)$_{0.9}$, which had a value of 30.3 ± 1.0 MPa probably as a result of the higher crosslink density due to the higher amount of saccharides found in ALnC. Materials using ALnP exhibit more brittle behavior, showing decreasing values of σ_m for higher R values, with the highest value of E recorded for VU-(ALnP-Pri)$_{0.9}$ at 837 ± 114 MPa. Since E in these samples is proportional to the mass fraction of respective acetoacetylated lignins, this is attributed to the fact that ALnP-based vitrimers have the highest amount of lignin content. Here, all mixtures display a narrow range of properties, attributed to the influence of the regular crosslinkers. These findings highlight the influence of the lignin source on the material's properties, which can be modified by adjusting the weight proportions of the different lignins, linkers, and amines. This influence of the amount of lignin crosslinkers was also found for materials synthesized from OSL and acetoacetylated poly(ethylene glycol) forming a vinylogous urethane with hexamethylene diamine linkers (lignin content varied from 30–50 wt%). Here, the E modulus increased from 0.2 ± 0.1 MPa with σ_m of 0.2 ± 0.1 MPa and ε_m values of 98% ± 10% with 30 wt% of lignin in the matrix up to 420 ± 30 MPa and with σ_m of 17.2 ± 0.7 MPa and ε_m values of 22 ± 3%, when using 50 wt% of lignin.[49] A detailed comparison of three vinylogous urethane vitrimer materials from OOSL, OSL and WSL is presented in Table S8,† including mechanical, rheological, and thermal properties of the samples. An excellent review on different lignin sources reviewing various dynamic covalent chemistries is provided by Karoki *et al.*, which lists values for E ranging from 0.2–85 MPa.[39]

Dynamic mechanical properties

Dynamic mechanical properties were further analyzed using dynamic mechanical analysis (DMA) and static stress relaxation experiments. Prior to all oscillatory experiments, amplitude sweep measurements were conducted at 110 °C to determine the linear viscoelastic regime (LVE) of the materials (Fig. 4a and S63, ESI†). An increase in the R-value reduces the number of dangling chains, as the amount of free amine functions decreases. This effect can be observed by higher values of the storage modulus in VU-(ALs-Pri)$_{0.6}$ and VU-(ALs-Pri)$_{0.5}$ compared to VU-(ALs-Pri)$_{0.4}$ in the LVE (Fig. S63a–c, ESI†). Maintaining the R-value at 0.6 and compounding with the linear chains of APPD enhances the elastic properties of VU-(ALs/APPD$_5$-Pri)$_{0.6}$. This process expands the LVE to higher values of shear strain γ for VU-(ALs/APPD$_{15}$-Pri)$_{0.6}$, while preserving the values of the storage modulus G' in the LVE. This is an initial indication of the powerful potential to precisely tune the properties of lignin vitrimers. The LVE range was observed between 0.001% and 1% for all lignosulfonate-based vitrimers. This range expands to higher values for higher APPD content and lower R-values. For the vitrimers produced from ALnC and ALnP, the LVE range is between 0.001% and 0.5%, following the same trend in the R-value as discussed before. VU-(ALnP-Pri)$_{0.8}$ and VU-(ALnP-Pri)$_{0.9}$ display a more rigid structure in the amplitude sweeps, showing breaking events after reaching the non-linear regions at 1% and 0.3%, respectively. This may be due to the more regular morphology (as seen in SEM), fewer impurities (as seen in EDX), and higher content of lignin in ALnP, which enhance the interactions between lignin moieties and therefore the arrangement of lignin fragments in the material, thereby increasing stiffness. Moreover, impurities such as saccharides in ALnC may enhance the toughness of these materials. Therefore, to prevent damage to the structure, all subsequent oscillatory measurements were performed within the LVE, using a deformation of 0.01%. Temperature-sweep measurements are displayed in Fig. 4b and S64, ESI.† The examined samples did not show a rubbery plateau in the examined temperature range of 150 °C to 0 °C but displayed a broad glass transition region. This suggests that the distribution of lignin moieties within the material is heterogeneous in size, leading to a broadening of the chain movement resolution in the tan(δ). This was also observed in the work of Liu *et al.* for alkali lignin, where Priamine™ 1075 was used as soft

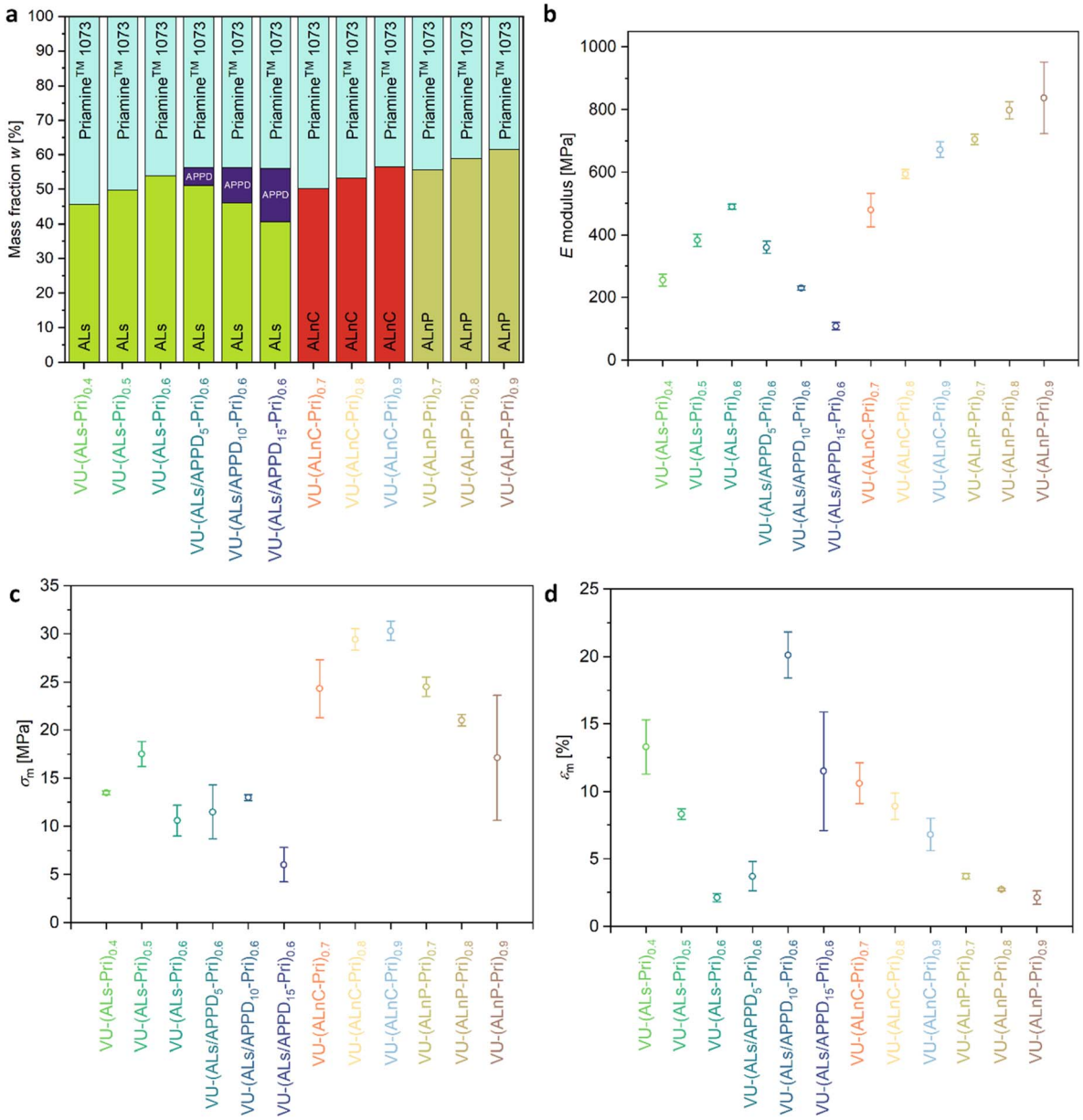

Fig. 3 (a) Mass fractions of the used building blocks of the lignin vitrimers with the acetoacetylated lignin species ALs, ALnC, and ALnP, respectively, the linear difunctional APPD, and the amount of Priamine™ 1073. (b–d) Tensile test data of the lignin vitrimers ($T = 23$ °C), (b) tensile modulus (E), (c) tensile strengths (σ_m), (d) elongation at ultimate stress (ε_m).

segment in a material crosslinked by hard and rigid lignin segments.[48] An interesting influence of the morphology of the used lignin type on the glass transition, displayed in Fig. 4c and S65,† can be found by comparing the temperature-sweep measurements of the lignosulfonates VU-(ALs-Pri) and VU-(ALs/APPD-Pri) with the materials VU-(ALnC-Pri) and VU-(ALnP-Pri). The ALs crosslinker results in a broad glass transition region, with a T_g at 30 °C for VU-(ALs-Pri)$_{0.4}$, which flattens and shifts to higher temperatures with increasing R-values. At 20 °C, the samples are in the glassy region, with storage moduli ranging from 85 MPa to 487 MPa. For the enzymatic lignin sources, ALnC and ALnP, a glass transition can be identified as a peak in tan(δ). The T_g shifts from 85 °C (VU-(ALnC-Pri)$_{0.7}$) to higher values with increasing R-values, resulting in a T_g of 110 °C for VU-(ALnC-Pri)$_{0.9}$. The purified enzymatic lignin exhibits even higher T_g values, demonstrating the same dependence on pending free amines within the material, with the T_g ranging from 115 °C for VU-(ALnP-Pri)$_{0.7}$ to 135 °C for VU-(ALnP-Pri)$_{0.9}$. This highlights the influence of the morphology of different lignin sources, as materials exhibit higher T_g values when they have a higher lignin content and fewer impurities like sulfonate groups in ALs-based materials, as discussed before. Interestingly, these materials, with broad T_gs, show stress-relaxation behavior even at temperatures as low as 120 °C. However, the T_g of the lignin particles can superimpose the stress-relaxation

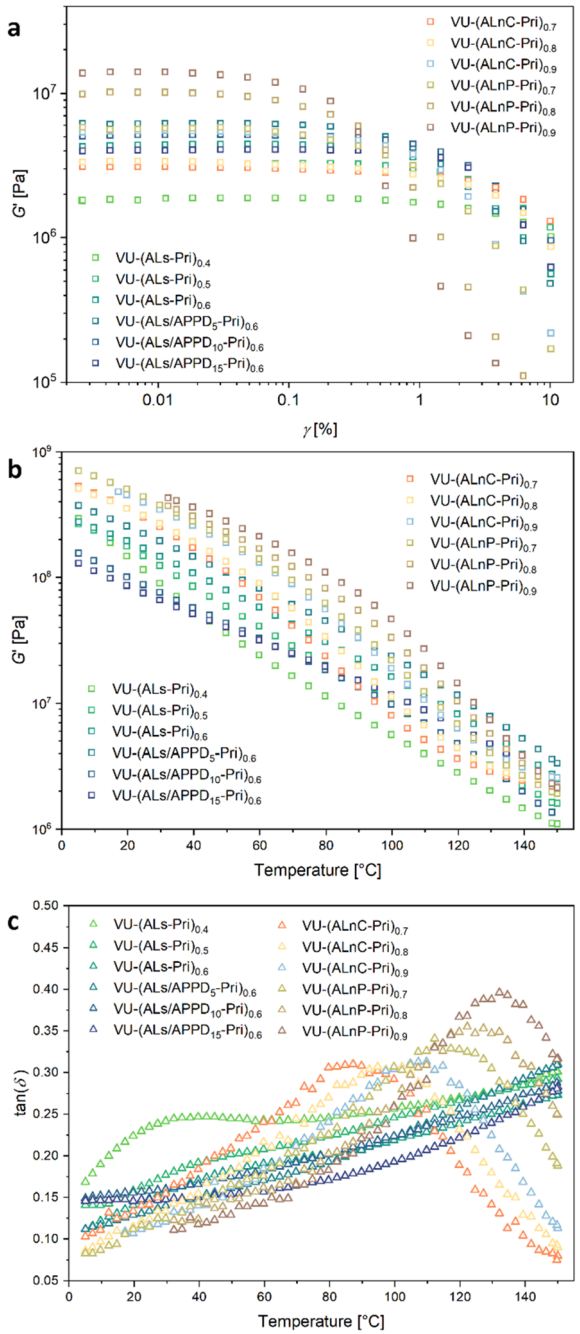

Fig. 4 DMA results of the lignin vitrimers based on lignosulfonate and enzymatic lignins (ω = 6.28 rad s^{-1}, F_N = 1 N). (a) Amplitude-sweep measurement results of the tested lignin vitrimers (T = 110 °C). (b and c) Temperature-sweep measurements of the lignin vitrimers (T = 150–0 °C, γ = 0.01%), (b) storage modulus G', (c) loss factor tan(δ).

behavior, potentially leading to inaccurate activation energy calculations.

Stress-relaxation properties

Stress-relaxation measurements were conducted on all lignin vitrimer materials to determine molecular network rearrangement. Vinylogous urethane bonds can exchange with free amines under thermal activation *via* a transamination reaction. As thermal energy increases, the rate of the bond exchanges also increases. Additionally, the structural and conformational properties of the material influence the dynamics of the free chains undergoing a molecular network rearrangement reaction. Commonly, the dependence of the stress-relaxation on the kinetics of dynamic exchange reactions in lignin-based vitrimers was proven by testing for the Arrhenius behavior using a single Maxwell model.[42,48,62] However, polymers, vitrimers, and organic composites like acetoacetylated lignin fragments should not be considered to be materials showing only a single relaxation, as they can display inhomogeneities and structural defects as well as show dependence from the T_g of the lignin, particularly if the thermal activation is close to the T_g.[63,64] A more realistic model that fits the data is the Kohlrausch–Williams–Watts (KWW) stretched exponential decay (ESI, eqn (S4)†).[7,47,50] A non-normalized version of the KWW model was used to calculate all parameters of the fit for the stress relaxation modulus $G(t)$. The stretching variable β is a measure for the uniformity of the exponential decay. A value of $\beta = 1$ indicates that the relaxation is described with a single relaxation time. The smaller the value, the broader is the distribution of relaxation times.[65] As a constrained condition, $G(t)$ is expected to be zero within experimental error at infinite time. In a first series of single-step deformation experiments of 1% deformation, the stress-relaxation modulus was measured as a function of time over a temperature range of 110 °C to 180 °C for all materials. The first criterion for stress-relaxation measurements is verifying if the initial relaxation modulus, G_0, remains nearly constant at different temperatures to confirm the assumption of an associative network rearrangement path. The values of G_0 in the range of 110–180 °C are shown in Fig. S66† and fulfill this criterion for the materials VU-(ALs-Pri)$_x$, VU-(ALs/APPD$_y$-Pri)$_x$. The materials VU-(ALnC-Pri)$_x$ and VU-(ALnP-Pri)$_x$ (Fig. S66b†) exhibit two different slopes in the straight lines connecting the values above and below 160 °C, suggesting a first indication of deviation from the expected stress-relaxation behavior, caused by T_g. Non-normalized stress-relaxation curves are presented alongside with the KWW function applied to the non-normalized stress relaxation data of the vitrimers VU-(ALs-Pri)$_x$, VU-(ALs/APPD$_y$-Pri)$_x$ VU-(ALnC-Pri)$_x$, and VU-(ALnP-Pri)$_x$ in Fig. S67.† The average relaxation times were calculated using eqn (S5).†[50,65] As listed in Table S9,† the stress relaxation results were well fit to stretched exponential decays for the materials VU-(ALs-Pri)$_x$, VU-(ALs/APPD$_y$-Pri)$_x$, and VU-(ALnC-Pri)$_{0.7}$, but result in high values for the averaged stress relaxation times for the respective materials VU-(ALnC-Pri)$_x$ and VU-(ALnP-Pri)$_x$. This demonstrates the influence of the high T_g values of ALnC and ALnP, also indicated by β values below 0.1. Therefore, these materials were excluded from the calculations of activation energies (E_a) for the transamination of the vinylogous urethane functions. In VU-(ALs-Pri)-based materials, the influence of the T_g appears less pronounced, as the softer matrix has a greater impact on the molecular network rearrangement, allowing for the calculation of E_as. Values of E_a for VU-(ALs-Pri)$_x$, VU-(ALs/APPD$_y$-Pri)$_x$, and VU-(ALnC-Pri)$_{0.7}$ were calculated by linear regression of the values of $\ln\langle\tau_r\rangle$ as a function of 1000/T in the

linear range of points between 110–180 °C (Fig. S68, ESI†). Calculated activation energies between 61.4–123 kJ mol^{-1} are typical values for transamination reactions.[58] Activation energies between 38–114 kJ mol^{-1} were calculated for OSL and OOSL and 134 kJ mol^{-1} for WSL, assuming a single relaxation.[47–49]

It has to be mentioned, that at temperatures of 170 °C and 180 °C slower stress relaxation was observed and also some measurements at 120 °C showed faster relaxation than the respective measurement at 130 °C, indicating measurement errors. The greater the influence of the harder lignin crosslinker segments and thus of the higher T_g, the greater becomes the influence of the limited segmental motion of the materials. This results in the spike in the Arrhenius plots for VU-(ALnC-Pri)$_{0.8}$, VU-(ALnC-Pri)$_{0.9}$, and all ALnP-based materials. The plot of the values of $\ln\langle\tau_r\rangle$ as a function of $1000/T$ displays a local maximum in the average stress-relaxation time in the region of the T_g. The KWW-fits calculate β values below 0.1, indicating a very broad distribution of relaxation times (ESI, Fig. S68(h–l) and ESI, Table S9†).

However, for these materials, the stress relaxations at 170 °C and 180 °C are particularly interesting for further investigations within this temperature range, as they appear to exhibit a linear relationship, suggesting that these materials could be processed at 180 °C. To investigate the potential stress-relaxation behavior of the material VU-(ALnC-Pri)$_x$ and VU-(ALnP-Pri)$_x$, additional stress relaxation measurements were conducted in the temperature range of 170–180 °C. In this temperature range, G_0 remains nearly constant across all materials, as displayed in Fig. S69.† A comparison of the different stress-relaxation behaviors of the materials VU-(ALs-Pri)$_{0.5}$ and VU-(ALnP-Pri)$_{0.7}$ is displayed in Fig. 5. The non-normalized stress-relaxation curves for VU-(ALnC-Pri)$_x$, and VU-(ALnP-Pri)$_x$ are shown together with the KWW function applied to the non-normalized stress relaxation data in Fig. S70.† The calculated values of β and $\langle\tau_r\rangle$ are listed in Table S10.† Next, the values of $\ln\langle\tau_r\rangle$ were plotted as a function of $1000/T$ in the linear range of points between 170–180 °C in Fig. S71, ESI,† showing linearity for VU-(ALnC-Pri)$_x$, and VU-(ALnP-Pri)$_{0.7}$. An increasing R-value for the materials VU-(ALnP-Pri)$_{0.8}$ and VU-(ALnP-Pri)$_{0.9}$ leads to the observation of increasing stress relaxation times at lower temperatures, deviating from linearity. As discussed before, the broad range of the T_g of the different materials influences the stress-relaxation behavior, leading to false assumptions of the activation energies and time-scales of the reprocessing. The calculated activation energies between 220–773 kJ mol^{-1} do not show values of stress-relaxation energies caused by transamination reactions, but are influenced by other relaxations in the materials. This is also highlighted by the deviation of the activation energy calculated for VU-(ALnC-Pri)$_{0.7}$, which shows an activation energy of 79.3 kJ mol^{-1} for the calculation between 120–180 °C and 220 kJ mol^{-1} for the calculation between 170–180 °C. These findings highlight the importance of using a KWW stretched exponential fit for stress-relaxation data of complex materials such as lignin vitrimers and to take the thermal properties such as the T_g of the monomers into account.

Recycling

The recycling of new sustainable materials is a key feature for a circular carbon economy. By recycling of lignin vitrimers, an industrial waste product can be used even after the first lifecycle by reprocessing and remolding, implementing green chemistry

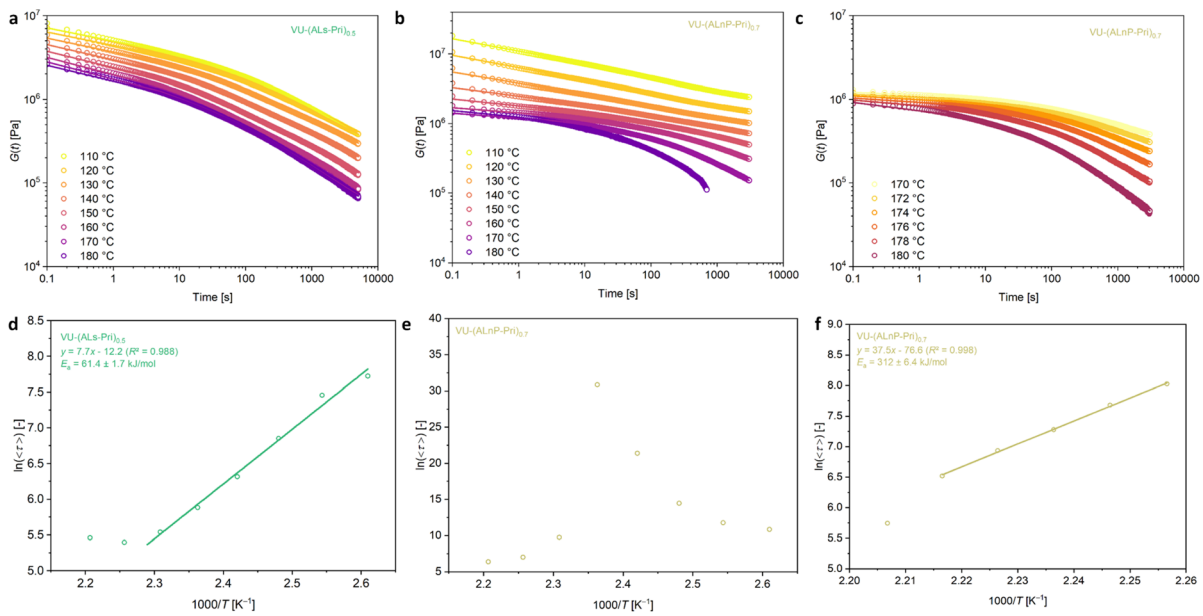

Fig. 5 Non-normalized stress-relaxation measurement ($\gamma = 1\%$, $F_N = 1$ N) between 110 °C and 180 °C of the material (a) VU-(ALs-Pri)$_{0.5}$ and (b) VU-(ALnP-Pri)$_{0.7}$. (c) Non-normalized stress-relaxation measurement ($\gamma = 1\%$, $F_N = 1$ N) between 170 °C and 180 °C of the material VU-(ALnP-Pri)$_{0.7}$. (d and e) Arrhenius plot of $\ln\langle\tau_r\rangle$ *versus* $1000/T$. For VU-(ALnP-Pri)$_{0.7}$, a non-linear plot (e) was found due to the high T_g of the lignin particles in the range of 110–180 °C. A linear stress-relaxation relation could be found for VU-(ALnP-Pri)$_{0.7}$ in the range of 170–180 °C (f).

principles towards a sustainable circular economy.[66,67] For this, exemplary samples of all materials were ground into a powder using a ball mill (1 min, 30 Hz, 23 °C) and remolded by heat compression (30 min, 20 kN, 180 °C) in five successive cycles. The results of the recycling experiments are displayed in Fig. 6. The integrity of the network properties after the recycling were reanalyzed after the fifth recycling step. Tensile testing results are listed in Table S11.† The properties of the reprocessed Ls-based material VU-(ALs-Pri)$_{0.5}$ were similar to the neat material with values of $E = 415 \pm 26.3$ MPa and $\sigma_m = 18.3 \pm 1.0$ MPa.

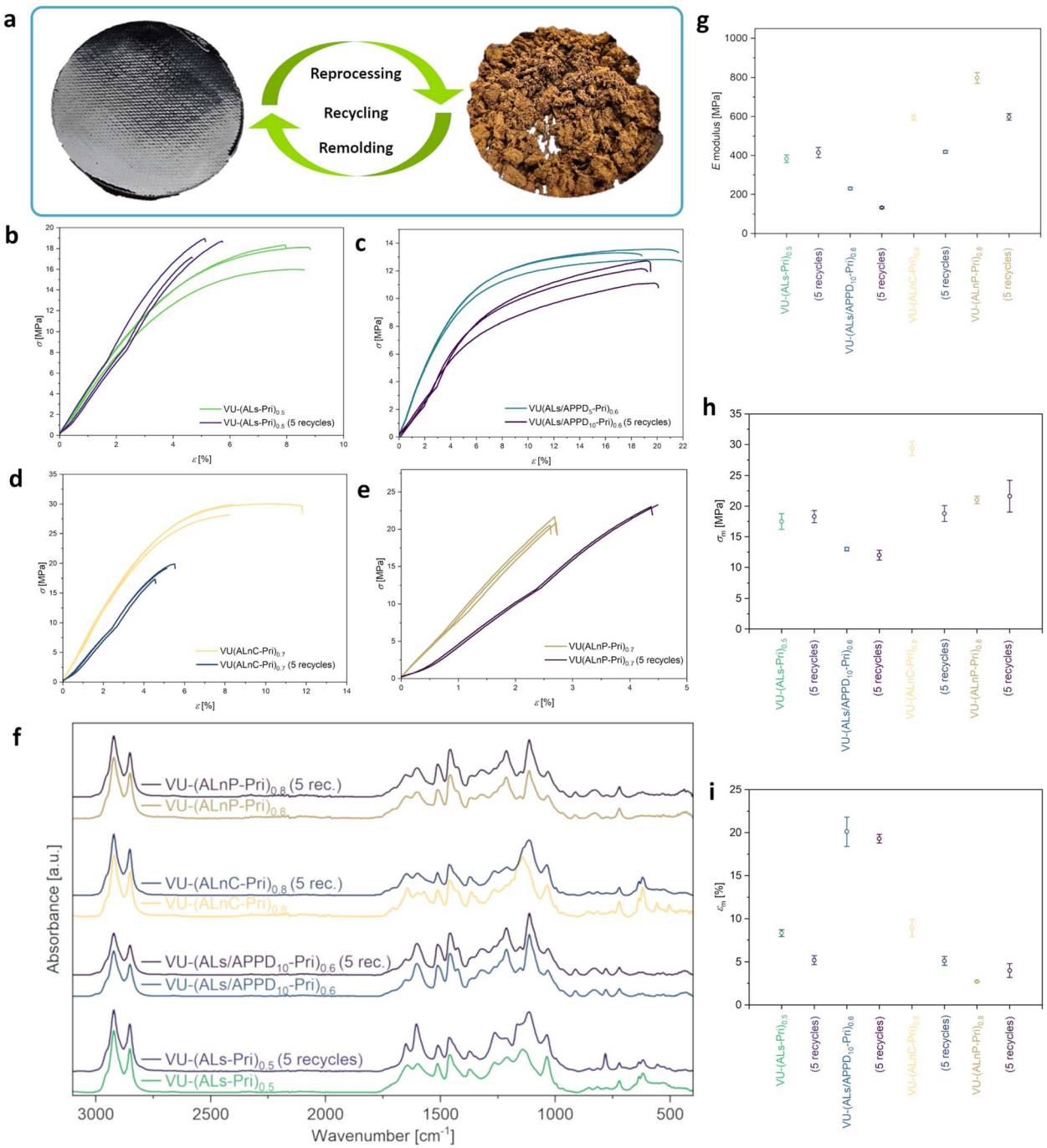

Fig. 6 (a) Illustration of the repetitive ball milling (1 min, $f = 30$ Hz, $T = 23$ °C) and reprocessing cycle through heat compression (30 min, 20 kN, 180 °C), showing a ground lignin vitrimer powder and a reprocessed vitrimer film. Stress–strain curves ($T = 23$ °C) of selected vitrimers VU-(ALs-Pri)$_{0.5}$ (b), VU-(ALs/APPD$_{10}$-Pri)$_{0.6}$ (c), VU-(ALnC-Pri)$_{0.8}$ (d) and VU-(ALnP-Pri)$_{0.8}$ (e) in comparison of the pristine and five times reprocessed specimens, showing different curves with overall similar material properties. (f) Repetitively measured ATR-FT-IR spectra show rather similar curve shapes of the pristine materials and after five times recycling procedure, measuring the characteristic stretching vibrations of the vinylogous urethane bond. (g–i) Tensile test data of the pristine and five times reprocessed lignin vitrimers ($T = 23$ °C), (g) E modulus, (h) tensile strengths (σ_m), (i) elongations at ultimate stress (ε_m).

The value of ε_m decreased from 8.3 ± 0.4% to 5.2 ± 0.5%, indicating an influence of the grinding process on the samples. In SEM and EDX measurements, displayed in Fig. S72–S75, ESI,† the structure of the cross-sections of the recycled vitrimers was analyzed. For VU-(ALs-Pri)$_{0.5}$ and VU-(ALs/APPD$_{10}$-Pri)$_{0.6}$, the distribution of sulfur-containing fragments appears homogeneous throughout the observed area. For VU-(ALs/APPD$_{10}$-Pri)$_{0.6}$, sulfur and sodium were also found in regions which only contained carbon and oxygen before the recycling, indicating an influence of the mechanical recycling on the structure by grinding and mixing. For the samples containing enzymatic lignin, SEM and EDX (Fig. S72–S75 and Tables S12–S15, ESI†) confirmed again a homogeneous structure. However, no influence of the recycling could be determined by these characterizations. As for the neat materials, again AFM measurements were carried out for the recycled materials, displayed in Fig. S76–S79, ESI.† After recycling, the films display a smoother surface, which could be due to a better mixture after consecutive grinding and remolding steps.

For tensile testing, the E modulus of the VU-(ALs/APPD$_{10}$-Pri)$_{0.6}$ decreased from 230 ± 6.0 MPa to 133 ± 5.9 MPa, indicating a degradation of the APPD linker molecules. However, the values of σ_m and ε_m were restored, which also shows the reprocessing potential of these compounds. Enzymatic lignin-based materials VU-(ALnC-Pri)$_{0.8}$ and VU-(ALnP-Pri)$_{0.8}$ displayed lower E moduli than the initial materials (797 MPa to 598 MPa and 594 MPa to 418 MPa), with VU-(ALnC-Pri)$_{0.8}$ also displaying ε_m decreased from 29.4 ± 1.1% to 18.8 ± 1.3%, also showing internal effects of low molecular weight compounds, which can also degrade during the milling and remolding steps.[68]

In comparison, for OSL, reprocessing was demonstrated by Sougrati *et al.* using a material with 40 wt% lignin, VU-40-400, which was cryo-ground in a coffee grinder. After three consecutive recycling cycles, the materials displayed a recovery of 71% of the initial stress at break, which was attributed to the alternation of the vitrimers structure. It was hypothesized, that not only dynamic bonds, but also bonds forming the network from lignin's bulky structure could be affected by the recycling process.[49] When recycling WSL Vitrimer-1 by Liu *et al.* by cutting the sample into pieces and recovering by hot pressing, after 4 consecutive cycles, the material properties were maintained, highlighting the influence of the mechanical process to recycle the lignin vitrimer and the amount of the linkers used.[48] This also becomes evident for a more recent work of Sougrati *et al.* on OOSL, where they obtained recycled materials without significant changes in chemical structure and mechanical properties for the vitrimer Ph-VU-600 with a lignin content of 46 wt% and a long PEG linker with a molar mass of 600 g mol^{-1}. This highlights the influence of a soft linker, resulting in an overall softer material (E = 2.4 ± 0.1 MPa), which facilitates preserving mechanical integrity after three reprocessing steps.[49]

DMA results of amplitude sweeps show a decrease in the LVE range for VU-(ALs-Pri)$_{0.5}$, VU-(ALs/APPD$_{10}$-Pri)$_{0.6}$, and VU-(ALnC-Pri)$_{0.8}$, whereas for VU-(ALnP-Pri)$_{0.8}$ it remained nearly the same, only the values of G' and G'' were lower (Fig. S80, ESI†). This may be explained by grinding of larger lignin fragments, resulting in samples with smoother surfaces, as seen in the AFM images. This can be observed in the temperature sweep data, showing overall decreased mechanical strength (Fig. S81, ESI†). As a result of better mixing and grinding of the polymer, a more homogeneous matrix could be achieved and the T_gs of VU-(ALs-Pri)$_{0.5}$ and VU-(ALs/APPD$_{10}$-Pri)$_{0.6}$ can be clearly determined in contrast to the pristine samples. For VU-(ALnC-Pri)$_{0.8}$ and VU-(ALnP-Pri)$_{0.8}$, the T_gs were shifted to higher temperatures (Fig. S82, ESI†). These results show that the internal morphology of the materials is affected by the reprocessing as shown by tensile testing. Stress-relaxation was investigated at four different temperatures, aligned with the previously determined temperature range for ALs, ALnC, and ALnP-based materials (Fig. S83, S84, Tables S16 and S17, ESI†). Except for VU-(ALs-Pri)$_{0.5}$, the materials show vitrimer-like stress-relaxation with increased characteristic relaxation times. Integrating APPD into the matrix of ALs-based vitrimers appears to enhance recyclability, as these materials continue to exhibit the characteristic relaxation behaviour of vitrimers even after recycling. The high activation energies do not display only the energy of transamination molecular network rearrangement but can be assigned to various relaxing effects, such as segmental motions.

UV-light absorbance

The suitability of materials for use as containers depends on their ability to absorb UV-light without heating or degradation.[69,70] When the vitrimer films were irradiated with UV-light (365 nm), no significant thermal effect was observed, other than an increase in the surface temperatures of both the sample and the PTFE sheet holding the sample. Three different time intervals (10 s, 60 s, and 300 s) were tested with an irradiation intensity of 69 mW cm^{-2}, showing no thermal heating effect of the neat vitrimer film (Fig. S85, ESI†).

Processing by injection molding

To demonstrate the suitability of lignin-based VU vitrimers for injection molding, the material VU-(ALnC-Pri)$_{0.7}$ was ground to a powder using a ball mill (25 °C, 30 Hz, 1 min) and subsequently filled into the injection molding cylinder at 250 °C, the mold was heated to 220 °C. Then, the specimens (Fig. 7a) were produced applying a pressure of 1000 bar for 45 s and a pressure of 100 bar for 20 s. After cooling, the specimens were extracted from the mold and tested by tensile testing (Fig. 7b), showing similar stress–strain curves and only slightly lower elastic moduli (406 MPa ± 16.2 MPa) as the heat compressed materials (479 MPa ± 53.2 MPa). This demonstrates the potential of processability of lignin-based VU-vitrimers not only by heat compression but also by injection molding, which could simplify the production of lignin-based materials by utilizing already existing large-scale production methods.

Durability tests and damping properties

To assess, if the vitrimer materials will be useful as recyclable damping materials, coatings, or containers that provide protection against environmental stress while offering a closed

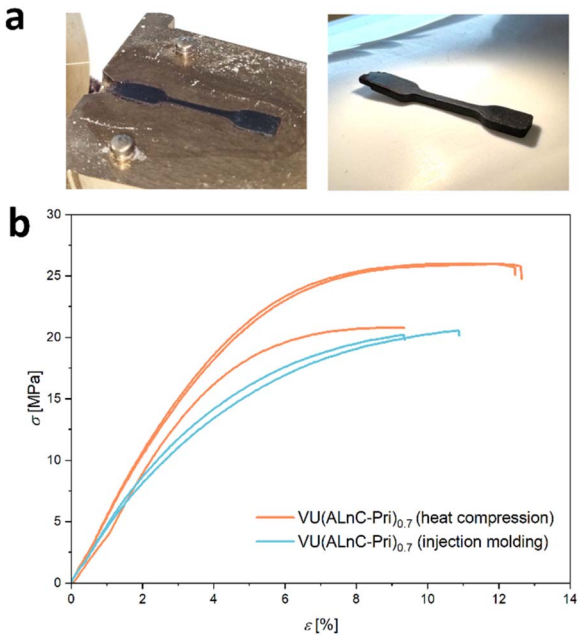

Fig. 7 (a) Pictures of the injection mold and the produced test specimen. (b) Comparison of the stress–strain curves specimens produced through heat compression and through injection molding.

carbon-cycle and industrial processing methods, durability tests were carried out.[71,72] The Shore-hardness of the injection molded VU-(ALnC-Pri)$_{0.7}$ was measured using a durometer device and an averaged value of 62D was measured in five measurement cycles. This proves the potential applicability as a protection against environmental mechanical stress and indicates durability.[73–75] The values are similar to lignin biocomposites, displaying values of 60D–80D, and display the influence of the mass loading of lignin.[76] Damping materials can effectively dissipate mechanical energy such as vibrations and absorb this energy while maintaining their structure.[77,78] As displayed in the previous chapter, the materials show a broad T_g due to a broad morphological size distribution allowing them to dissipate energy. A durability test was carried out with a square-shaped sample of VU-(ALnP-Pri)$_{0.7}$, applying a tensile-force of 50 N in an oscillating experiment with 1000 repetitive cycles of force and relaxation. The consecutive cycles are displayed in Fig. S86, ESI.† Fatigue can occur due to dynamic loading at stress amplitudes below the fracture strength. The material displayed no permanent deformation, cracks or material fatigue, indicating resistance against frequent vibrations. However, the elongation increased in the first 700 cycles by 33%, reaching a plateau value, indicating a quasi-stationary state.

Conclusions

A series of vinylogous urethane vitrimers derived under mild conditions from new lignin sources using lignosulfonate and enzymatic lignin (Lignova Crude™ and Lignova Pure™) is studied. These materials represent a promising class of tougher, greener, and sustainable vitrimers, characterized by strong mechanical properties, such as an elastic modulus of up to 0.83 GPa. Acetoacetylation using TBAA was performed in DMSO as a one-step bulk reaction. Subsequently, polymerization of lignin-based acetoacetates with a bio-based amine and an acetoacetylated polyol was carried out in a non-toxic water/acetone mixture. This process yielded vitrimer films after consecutive ball milling and remolding in a heat compression mold. The materials demonstrate stability against solvents, such as water and acetone, as indicated by swelling tests. Additionally, they exhibit high thermal stability, with a $T_{5\%}$ ranging from 272–307 °C, enhancing the thermal properties of the raw lignins. Twelve lignin vitrimers have been synthesized and compared regarding their morphology and mechanical properties, showing elastic moduli of 108–837 MPa, tensile strengths of 6.0–30.3 MPa, and elongations at ultimate stress of 2.1–20.1%. In general, vitrimers based on lignosulfonate were less homogeneous as observed by optical and scanning electron microscopy. They showed less tensile strength than vitrimers based on LnC and LnP. This results from the higher degree of impurities, heterogeneity, and dispersity of lignosulfonate. Stress-relaxation was investigated in two different temperature regimes, depending on the lignin resource used. The measurements were fitted using the Kohlrausch–Williams–Watts stretched exponential decay function, highlighting the importance of taking several relaxation phenomena (segmental motion and transamination reaction) into account for stress relaxation and calculation of activation energies. Furthermore, the materials allow for thermomechanical reprocessing through grinding and remolding, displaying the potential for closed-loop recycling of a waste product resource. The material properties were measured and compared after five successive grinding and remolding steps, highlighting the reprocessability, which is affected by the alteration of the inner structure of the materials. In addition, the materials display interesting optical properties such as blocking of UV-light, good Shore D hardness, and resistance against fatigue. Since mainly soft, elastomeric lignin-based vitrimers were reported before, focusing on organosolv lignin and Kraft lignin, this work contributes to the development of tough lignin vitrimers from waste-wood lignosulfonate lignin and enzymatic lignin with a high lignin content, and gives an in-depth investigation of mechanical and stress-relaxation properties, and introducing new processing methods such as injection molding for vinylogous urethane lignin vitrimers.

Data availability

Data is available upon reasonable request from the authors.

Author contributions

F. C. K. and N. S. contributed equally to this work. F. C. K., N. S., and V. A.: conceptualization; F. C. K. and N. S.: methodology, investigation, data curation, formal analysis, validation, visualization, and experiments; V. A.: supervision and resources; F.

C. K. and N. S.: writing – the original draft; F. C. K., N. S., and V. A.: writing – review and editing.

Conflicts of interest

There are no conflicts to declare.

Acknowledgements

The authors gratefully acknowledge financial support from the German Research Foundation (DFG) *via* SFB986 "M3," subproject A2. The authors would like to thank Fibenol OÜ, especially Kait Kaarel Puss, for providing the lignin samples and the friendly correspondence. The authors acknowledge the NMR division of the chemistry department at Universität Hamburg (UHH) with a special thanks to Claudia Wontorra for conducting the ^{31}P NMR measurements. We thank Robert Schön of the EM division for capturing the SEM images. The authors would like to address special thanks to Martin Kehden who conducted all DSC and TGA measurements. We thank Marvin Groß (OM), the MS division, Andreas Meyer (AFM), and Birgit Hankiewicz (DLS). This open access publication was funded by the University of Hamburg as part of the TIB-RSC-Platinum agreement with the Royal Society of Chemistry.

References

1 M. Calisto Friant, W. J. V. Vermeulen and R. Salomone, *Circ. Econ. Sustainability*, 2023, **4**, 23–42.
2 J. G. Rosenboom, R. Langer and G. Traverso, *Nat. Rev. Mater.*, 2022, **7**, 117–137.
3 M. Tschulkow, M. Pizzol, T. Compernolle, S. Van den Bosch, B. Sels and S. Van Passel, *Resour., Conserv. Recycl.*, 2024, **204**, 107466.
4 R. Shorey, A. Salaghi, P. Fatehi and T. H. Mekonnen, *RSC Sustainability*, 2024, **2**, 804–831.
5 P. Haida, S. Chirachanchai and V. Abetz, *ACS Sustainable Chem. Eng.*, 2023, **11**(22), 8350–8361.
6 C. Li, B. Ju and S. Zhang, *Cellulose*, 2021, **28**, 2879–2888.
7 L. Sougrati, A. Duval and L. Avérous, *J. Mater. Chem. A*, 2025, **13**, 4921–4939.
8 A. Duval, W. Benali and L. Averous, *ChemSusChem*, 2025, **18**, e202401480.
9 M. Bilal, S. A. Qamar, M. Qamar, V. Yadav, M. J. Taherzadeh, S. S. Lam and H. M. N. Iqbal, *Biomass Convers. Biorefin.*, 2022, **14**, 4457–4483.
10 J. Becker and C. Wittmann, *Biotechnol. Adv.*, 2019, **37**, 107360.
11 F. José Borges Gomes, R. E. de Souza, E. O. Brito and R. C. Costa Lelis, *J. Appl. Biotechnol. Bioeng.*, 2020, 100–105, DOI: **10.15406/jabb.2020.07.00222**.
12 L. Dessbesell, M. Paleologou, M. Leitch, R. Pulkki and C. Xu, *Renewable Sustainable Energy Rev.*, 2020, **123**, 109768.
13 D. D. S. Argyropoulos, C. Crestini, C. Dahlstrand, E. Furusjo, C. Gioia, K. Jedvert, G. Henriksson, C. Hulteberg, M. Lawoko, C. Pierrou, J. S. M. Samec, E. Subbotina, H. Wallmo and M. Wimby, *ChemSusChem*, 2023, **16**, e202300492.
14 M. Y. Balakshin, E. A. Capanema, I. Sulaeva, P. Schlee, Z. Huang, M. Feng, M. Borghei, O. J. Rojas, A. Potthast and T. Rosenau, *ChemSusChem*, 2021, **14**, 1016–1036.
15 J. J. Liao, N. H. A. Latif, D. Trache, N. Brosse and M. H. Hussin, *Int. J. Biol. Macromol.*, 2020, **162**, 985–1024.
16 Y. Yang, Y. Guan, C. Li, T. Xu, L. Dai, J. Xu and C. Si, *Adv. Compos. Hybrid Mater.*, 2024, **7**, 61.
17 C. Libretti, L. Santos Correa and M. A. R. Meier, *Green Chem.*, 2024, **26**, 4358–4386.
18 N. I. Jeffri, N. F. Mohammad Rawi, M. H. Mohamad Kassim and C. K. Abdullah, *Int. J. Biol. Macromol.*, 2024, **274**, 133506.
19 M. J. Getahun, B. B. Kassie and T. S. Alemu, *Process Biochem.*, 2024, **145**, 261–287.
20 M. T. Munir, M. Naqvi, B. Li, R. Raza, A. Khan, S. A. A. Taqvi and A.-S. Nizami, *J. Energy Storage*, 2024, **82**, 110477.
21 P. D'Arrigo, L. A. M. Rossato, A. Strini and S. Serra, *Molecules*, 2024, **29**, 442.
22 S. Behera, S. Mohapatra, B. C. Behera and H. Thatoi, *Crit. Rev. Biotechnol.*, 2024, **44**, 774–794.
23 R. Priyadarshi, T. Ghosh, S. D. Purohit, V. Prasannavenkadesan and J.-W. Rhim, *J. Cleaner Prod.*, 2024, **469**, 143151.
24 M. Mujtaba, L. Fernandes Fraceto, M. Fazeli, S. Mukherjee, S. M. Savassa, G. Araujo de Medeiros, A. do Espírito Santo Pereira, S. D. Mancini, J. Lipponen and F. Vilaplana, *J. Cleaner Prod.*, 2023, **402**, 136815.
25 L. Sougrati, A. Duval and L. Avérous, *Mater. Sci. Eng., R*, 2024, **161**, 100882.
26 G. F. Bass and T. H. Epps, *Polym. Chem.*, 2021, **12**, 4130–4158.
27 R. Grappa, V. Venezia, L. Basta, M. L. Alfieri, L. Panzella, M. Verrillo, B. Silvestri, M. Commodo, G. Luciani and A. Costantini, *ACS Sustainable Chem. Eng.*, 2024, **12**, 10653–10664.
28 L.-Y. Zhan, P. Li, Y.-D. Li, Y. Ran and J.-B. Zeng, *Eur. Polym. J.*, 2025, **227**, 113749.
29 T. Aro and P. Fatehi, *ChemSusChem*, 2017, **10**, 1861–1877.
30 T. Tang, J. Fei, Y. Zheng, J. Xu, H. He, M. Ma, Y. Shi, S. Chen and X. Wang, *ChemistrySelect*, 2023, **8**, e202204941.
31 A. Khajeh, Z. Nazari, M. Movahedrad and A. H. Vakili, *Sci. Total Environ.*, 2024, **943**, 173500.
32 J. Köhnke, N. Gerlinger, B. Prats-Mateu, C. Unterweger, P. Solt, A. Mahler, E. Schwaiger, F. Liebner and W. Gindl-Altmutter, *BioResources*, 2019, **14**, 1091–1109.
33 G. Unkelbach and T. Hirth, *EFB Bioeconomy J.*, 2022, **2**, 100036.
34 M. A. Lucherelli, A. Duval and L. Avérous, *Prog. Polym. Sci.*, 2022, **127**, 101515.
35 D. Montarnal, M. Capelot, F. Tournilhac and L. Leibler, *Science*, 2011, **334**, 965–968.
36 C. Taplan, M. Guerre, J. M. Winne and F. E. Du Prez, *Mater. Horiz.*, 2020, **7**, 104–110.
37 W. Denissen, J. M. Winne and F. E. Du Prez, *Chem. Sci.*, 2016, **7**, 30–38.
38 J. M. Winne, L. Leibler and F. E. Du Prez, *Polym. Chem.*, 2019, **10**, 6091–6108.

39 P. K. Karoki, S. Zhang, Y. Pu and A. J. Ragauskas, *Mater. Adv.*, 2024, **5**, 7075–7096.
40 Y. Du and D. Wang, *ACS Appl. Mater. Interfaces*, 2024, **16**, 41551–41561.
41 A. Moreno, M. Morsali and M. H. Sipponen, *ACS Appl. Mater. Interfaces*, 2021, **13**, 57952–57961.
42 J. Liu and K. V. Bernaerts, *J. Mater. Chem. A*, 2024, **12**, 2959–2973.
43 W. Zhao, Z. Liang, Z. Feng, B. Xue, C. Xiong, C. Duan and Y. Ni, *ACS Appl. Mater. Interfaces*, 2021, **13**, 28938–28948.
44 W. Zhuo, X. Luo, H. Yan, L. Shuai and Z. Wu, *Int. J. Biol. Macromol.*, 2025, 141550, DOI: **10.1016/j.ijbiomac.2025.141550**.
45 P. Haida and V. Abetz, *Macromol. Rapid Commun.*, 2020, **41**, e2000273.
46 E. M. Krall, E. M. Serum, M. P. Sibi and D. C. Webster, *Green Chem.*, 2018, **20**, 2959–2966.
47 L. Sougrati, A. Duval and L. Averous, *ChemSusChem*, 2023, **16**, e202300792.
48 J. Liu, A. Pich and K. V. Bernaerts, *Green Chem.*, 2024, **26**, 1414–1429.
49 L. Sougrati, A. Duval and L. Avérous, *Chem. Eng. J.*, 2025, **511**, 162201.
50 L. Li, X. Chen, K. Jin and J. M. Torkelson, *Macromolecules*, 2018, **51**, 5537–5546.
51 X. Meng, C. Crestini, H. Ben, N. Hao, Y. Pu, A. J. Ragauskas and D. S. Argyropoulos, *Nat. Protoc.*, 2019, **14**, 2627–2647.
52 A. Stücker, J. Podschun, B. Saake and R. Lehnen, *Anal. Methods*, 2018, **10**, 3481–3488.
53 A. Granata and D. S. Argyropoulos, *J. Agric. Food Chem.*, 1995, **43**, 1538–1544.
54 P. Haida, G. Signorato and V. Abetz, *Polym. Chem.*, 2022, **13**, 946–958.
55 Y. Archipov, D. S. Argyropoulos, H. I. Bolker and C. Heitner, *J. Wood Chem. Technol.*, 1991, **11**, 137–157.
56 J. Ruwoldt, *Surfaces*, 2020, **3**, 622–648.
57 M. Li, C. G. Yoo, Y. Pu and A. J. Ragauskas, *ACS Sustainable Chem. Eng.*, 2017, **6**, 1265–1270.
58 W. Denissen, G. Rivero, R. Nicolaÿ, L. Leibler, J. M. Winne and F. E. Du Prez, *Adv. Funct. Mater.*, 2015, **25**, 2451–2457.
59 J. D. Zwilling, X. Jiang, F. Zambrano, R. A. Venditti, H. Jameel, O. D. Velev, O. J. Rojas and R. Gonzalez, *Green Chem.*, 2021, **23**, 1001–1012.
60 B. Wang, D. Sun, H.-M. Wang, T.-Q. Yuan and R.-C. Sun, *ACS Sustainable Chem. Eng.*, 2018, **7**, 2658–2666.
61 C. Miao and W. Y. Hamad, *J. Appl. Polym. Sci.*, 2016, **134**, 44669.
62 G. Zhang, C. Tian, H. Chu, J. Liu, B. Guo and L. Zhang, *J. Mater. Chem. A*, 2023, **11**, 25356–25367.
63 T.-W. Lin, B. Mei, S. Dutta, K. S. Schweizer and C. E. Sing, *Macromolecules*, 2025, **58**, 1481–1497.
64 X. Cui, Y. Luo, Y. Yang and P. Tang, *Macromolecules*, 2025, **58**, 1898–1911.
65 A. Dhinojwala, J. C. Hooker and J. M. Torkelson, *J. Non-Cryst. Solids*, 1994, **172–174**, 286–296.
66 T. L. Chen, H. Kim, S. Y. Pan, P. C. Tseng, Y. P. Lin and P. C. Chiang, *Sci. Total Environ.*, 2020, **716**, 136998.
67 P. Anastas and N. Eghbali, *Chem. Soc. Rev.*, 2010, **39**, 301–312.
68 F. Gamardella, S. De la Flor, X. Ramis and A. Serra, *React. Funct. Polym.*, 2020, **151**, 104574.
69 A. I. Quilez-Molina, U. Chandra Paul, D. Merino and A. Athanassiou, *ACS Sustainable Chem. Eng.*, 2022, **10**, 15402–15413.
70 S. Shankar, J. P. Reddy and J. W. Rhim, *Int. J. Biol. Macromol.*, 2015, **81**, 267–273.
71 O. Yu and K. H. Kim, *Appl. Sci.*, 2020, **10**, 4626.
72 B. Krishnakumar, A. Pucci, P. P. Wadgaonkar, I. Kumar, W. H. Binder and S. Rana, *Chem. Eng. J.*, 2022, **433**, 133261.
73 N. L. Kapuge Dona, P. Y. Sauceda-Oloño and R. C. Smith, *J. Polym. Sci.*, 2024, **63**, 789–799.
74 J. M. Lang, U. M. Shrestha and M. Dadmun, *Front. Energy Res.*, 2018, **6**, 4.
75 C.-W. Chen, H.-I. Mao, H.-K. Lee, J.-Y. Chou and S.-P. Rwei, *J. Polym. Environ.*, 2023, **32**, 621–631.
76 M. Goliszek and B. Podkościelna, *Physicochem. Probl. Miner. Process.*, 2019, **55**, 1375–1381.
77 M. A. Shaid Sujon, A. Islam and V. K. Nadimpalli, *Polym. Test.*, 2021, **104**, 107388.
78 Y. Li, H. Feng, J. Xiong and L. Li, *Materials*, 2024, **17**, 5062.